The calcium sensor synaptotagmin-1 is critical for phasic axonal dopamine release in the striatum and mesencephalon, but is dispensable for basic motor behaviors in mice

Benoît Delignat-Lavaud[1,2,3], Jana Kano*[1,2,3], Charles Ducrot*[1,2,3], Ian Massé[4], Sriparna Mukherjee[1,2,3], Nicolas Giguère[1,2,3], Luc Moquin[5], Catherine Lévesque[6], Samuel Burke Nanni[1,2,3], Marie-Josée Bourque[1,2,3], Pedro Rosa-Neto[5], Daniel Lévesque[6], Louis De Beaumont[4], Louis-Éric Trudeau[1,2,3]

[1]Department of Pharmacology and Physiology, Faculty of Medicine, Université de Montréal
[2]Department of Neurosciences, Faculty of Medicine, Université de Montréal
[3]CNS Research Group (GRSNC),
[4]Hôpital du Sacré-Cœur-de-Montréal, CIUSSS NIM, Université de Montréal,
[5]The Douglas Research Centre, McGill University,
[6]Faculty of Pharmacy, Université de Montréal
Montréal, QC, Canada
*Equal contribution

Corresponding author:
Dr. Louis-Éric Trudeau
Department of pharmacology and physiology
Faculty of Medicine
Université de Montréal
louis-eric.trudeau@umontreal.ca
514-343-5692

Summary

Midbrain dopamine (DA) neurons, a population of cells that are critical for motor control, motivated behaviors and cognition, release DA via an exocytotic mechanism from both their axonal terminals and their somatodendritic (STD) compartment. In Parkinson's disease (PD), it is striking that motor dysfunctions only become apparent after extensive loss of DA innervation. Although it has been hypothesized that this resilience is due to the ability of many motor behaviors to be sustained through a basal tone of DA and diffuse transmission, experimental evidence for this is limited. Here we conditionally deleted the calcium sensor synaptotagmin-1 (Syt1) in DA neurons (cKO^{DA} mice) to abrogate most activity-dependent axonal DA release in the striatum and mesencephalon, leaving STD DA release intact. Strikingly, Syt1 cKO^{DA} mice showed intact performance in multiple unconditioned DA-dependent motor tasks, suggesting that activity-dependent DA release is dispensable for such basic motor functions. Basal extracellular levels of DA in the striatum were unchanged, suggesting that a basal tone of extracellular DA is sufficient to sustain basic movement. We also found multiple adaptations in the DA system of cKO^{DA} mice, similar to those happening at early stages of PD. Taken together, our findings reveal the striking resilience of DA-dependent motor functions in the context of a near-abolition of phasic DA release, shedding new light on why extensive loss of DA innervation is required to reveal motor dysfunctions in PD.

Keywords: dopamine, exocytosis, synaptotagmin, somatodendritic, movement

Introduction

The neuromodulator dopamine (DA) plays a key role in motor control, motivated behaviors and cognition *(Schultz, 2007; Surmeier et al., 2014)*. Blockade of DA receptors severely impairs most motor behaviors *(Hauber, 1996)* and a severe loss of DA in the striatum and other brain regions leads to the characteristic motor dysfunctions of Parkinson's disease (PD). It is striking that in PD, motor dysfunctions only appear when the striatum is severely denervated and that DA replacement therapy with L-DOPA is able to restore motor functions by boosting DA production in the remaining, sparse DA axonal fibers *(Mercuri and Bernardi, 2005)*. Such observations are puzzling and ill-understood and suggest the possibility that a minimal basal tone of DA, coupled with adaptations to the DA system to boost its sensitivity, are sufficient to maintain motor functions *(Golden et al., 2013)*.

Compatible with such observations, DA is thought to act in the brain as a neuromodulator involved in a form of "volume transmission" and not as a point-to-point fast neurotransmitter *(Descarries et al., 1996; Antonopoulos et al., 2002; Descarries et al., 2008; Ducrot et al., 2021)*. DA release occurs not only from axon terminals in the vast axonal arbors of DA neurons, but also from the neurons' somatodendritic (STD) compartment *(Rice and Patel, 2015)*. The molecular machinery underlying exocytotic DA release from terminals *(Mendez et al., 2011; Liu et al., 2018; Banerjee et al., 2020a; Liu et al., 2021)* or dendrites *(Bergquist et al., 2002; Fortin et al., 2006; Hikima et al., 2021; Mendez et al., 2011; Ovsepian and Dolly, 2011; Rice and Patel, 2015)* is presently fragmentary. Discoveries on such mechanisms are likely to lead to a better understanding of the functions and connectivity of all classes of modulatory neurons.

Vesicular exocytosis requires the concerted action of SNARE proteins and calcium sensors from the synaptotagmin family (Syt) *(Sudhof, 2004)*. Of the 17 Syt isoforms identified

so far, only Syt1, 2, 3, 5, 6, 7, 9, and 10 have been reported to bind calcium and drive vesicular fusion *(Andrews and Chakrabarti, 2005)*. Syt1, 2, and 9 were confirmed as calcium sensors for fast synaptic neurotransmitter release from axon terminals *(Xu et al., 2007)*. Syt1 was first shown to play a key role in axonal DA release in primary DA neurons *(Mendez et al., 2011)* in which it is present at both synaptic and non-synaptic terminals *(Ducrot et al., 2021)*, but most likely absent from dendrites *(Mendez et al., 2011)*. Recent work has confirmed and extended this finding in the intact brain by showing that Syt1 is essential for evoked DA release *(Banerjee et al., 2020b)*. Syt4 and Syt7 were recently shown to control STD DA release, suggesting a distinct molecular machinery compared to axonal DA release *(Mendez et al., 2011; Delignat-Lavaud et al., 2021)*.

Here, we defined the consequence of loss of Syt1 in DA neurons by evaluating the impact of this deletion on DA-dependent behaviors and by characterizing the selective roles of Syt1 in axonal and STD DA release. We find that basic unconditioned motor functions are intact in mice lacking Syt1 in DA neurons (Syt1 cKO^{DA}). Combined with our observations that loss of Syt1 leads to extensive loss of axonal DA release in the striatum, to partial loss of DA release in the mesencephalon and to unaltered extracellular DA levels in the striatum and mesencephalon, our findings suggest that basal unconditioned motor functions in rodents only require the maintenance of a basal tone of extracellular DA largely independent of Syt1-dependent phasic release. We hypothesize that this situation is very similar to pre-symptomatic stages of PD and sheds light on the surprising resilience of motor functions after extensive loss of evoked DA.

Methods

Animal model

The Syt1-floxed mouse line (Syt1$^{lox/lox}$) was obtained from Dr. Schneggenburger who rederivated the Syt1$^{tm1a(EUCOMM)Wtsi}$ *(EMMA, Monterotondo, Italy; EM06829; RRID:MGI_5450372)* strain with a C57Bl6 background carrying a constitutively expressing FLP gene in order to remove the Frt-flanked lacZ/neo insert *(Kochubey et al., 2016)*. We then crossed the Syt1$^{lox/lox}$ mice with B6.SJL-Slc6a3$^{tm1.1(cre)Bkmm}$/J; DATIRES-Cre mice *(The Jackson Laboratory, stock 006660, USA)*, driving expression of the cre recombinase under the control of the DAT promoter, resulting in the selective deletion of *Syt1* alleles in DA neurons (**Fig. 1A**). Syt1-floxed/DAT$^{IRES-cre}$ mice were bred from heterozygous crosses to generate Syt1 conditional knockout in DA neurons (cKO^{DA}), heterozygotes and wild-type animals, referred in the manuscript as Syt1$^{-/-}$, Syt1$^{+/-}$ and Syt1$^{+/+}$ respectively. Genotyping for Syt1 cKO^{DA} mice was determined using specific primers to target the *Syt1*-floxed alleles - Syt1^{lox} forward: GATTCATGATGTCACTGAATCCTATGC and Syt1^{lox} reverse CTGGCAAGTAGCTTAGTGAGTC. Experiments were performed blind with regards to animal genotype. All procedures involving animals and their care were conducted in accordance with the Guide to care and use of Experimental Animals of the Canadian Council on Animal Care. The experimental protocols were approved by the animal ethics committees of the Université de Montréal. For microdialysis experiment, the study was approved by the animal care committee of the research center of the Hôpital du Sacré-Cœur de Montréal (CIUSSS NIM). Housing was at a constant temperature (21°C) and humidity (60%), under a fixed 12h light/dark cycle, with food and water available ad libitum.

Virus injections

6-7 week-old cKO^{DA} or $Syt1^{lox/lox}$ mice were anesthetized with isoflurane *(Aerrane; Baxter, Deerfield, IL, USA)* and fixed on a stereotaxic frame *(Stoelting,Wood Dale, IL, USA).* A small hole was drilled in the exposed skull and a 10 µl Hamilton syringe connected to a borosilicate injection micropipette pulled using a P-2000 puller *(Sutter Instrument)* coupled with a Quintessential Stereotaxic Injector *(Stoelting)* were used for the injections. For virally induced Syt1 KO, a AAV9-TH-cre-myc-2A-fusion-red virus (2.1E+13vg/ml) and AAV9-TH-fusion-red-Sv40 (1.99E+13vg/ml) control virus *(kindly provided by Dr. James Surmeier)* were injected bilaterally to $Syt1^{lox/lox}$ mice at the following injection coordinates [AP (anterior–posterior; ML (medial–lateral); DV (dorsal-ventral), from bregma]: AP -2.8 mm; ML + and – 0.9 mm; DV -4.3 mm and AP -3.2 mm; ML + and – 1.5 mm; DV -4.2 mm (0.5 µL per sites at a rate of 0.25 µL/min, for a total of 2 µl per mice), in order to infect neurons in the entire ventral mesencephalon. For optogenetic experiments, a pAAV-syn-ChR2-eYFP-Kv plasmid was purchased *(Addgene plasmid # 89256, USA, originally from McLean Bolton)*, modified to insert a double-floxed inverse open reading frame (DIO) and packaged into an AAV2/5 backbone. The AAV2/5-hsyn-DIO-ChR2-eYFP-Kv (6.2 *$x10^{12}$ vg/mL, Neurophotonics Québec, CANADA)* virus or a AAV5-EF1a-DIO-hChR2(H134R)-eYFP *($4.2x10^{12}$ vg/mL, UNC GTC Vector core, USA)* control virus were injected with the same protocol as above to infect the entire mesencephalon of $Syt1^{+/+}$ and $Syt1^{-/-}$ mice. Each virus was diluted (1:3) with sterile saline solution and kept on ice prior injections. Animals recovered in their home cage and were closely monitored for 3 days. The brains were collected for FCSV and immunohistochemistry 3-4 weeks after injections. For FSCV experiment success of the injections was visually validated each time during the slicing of the brains by visualizing the presence of the eYFP reporter.

Brain slices preparation

Acute brain slices from 10-12-week-old male or female cKO^{DA} mice were used for all fast scan cyclic voltammetry (FSCV) recordings. When possible, matched pairs of $Syt1^{+/+}$ and $Syt1^{+/-}$/$Syt1^{-/-}$ mice were used on each experimental day. The animals were anesthetized with halothane, decapitated and the brain quickly harvested. Next, the brain was submersed in ice-cold oxygenated artificial cerebrospinal fluid (aCSF) containing (in mM): NaCl (125), KCl (2.5), KH_2PO_4 (0.3), $NaHCO_3$ (26), glucose (10), $CaCl_2$ (2.4), $MgSO_4$ (1.3) and coronal striatal and/or midbrain brain slices of 300 µm thickness were prepared with a Leica VT1000S vibrating blade microtome. Once sliced, the tissue was transferred to oxygenated aCSF at room temperature and allowed to recover for at least 1h. For recordings, slices were placed in a custom-made recording chamber superfused with aCSF at 1 ml/min and maintained at 32°C with a TC-324B single channel heater controller *(Warner Instruments, USA)*. All solutions were adjusted at pH 7.35-7.4, 300 mOsm/kg and saturated with 95% O_2-5% CO_2 at least 30 min prior to each experiment.

Fast Scan Cyclic Voltammetry

Electrically or optically evoked DA release was measured by FSCV using a 7 µm diameter carbon-fiber electrode placed into the tissue ~100 µm below the surface. A bipolar electrode *(Plastics One, Roanoke, VA, USA)* or an optical fiber connected to a 470 nm wavelength LED was placed ~200 µm away from the recording site. Carbon-fiber electrodes *(Goodfellow Cambridge Limited, UK)* of 7 µm in diameter were aspirated into ethanol-cleaned glass capillaries *(1.2 mm O.D., 0.68 mm I.D., 4 inches long; World Precision Instruments, FL, USA)*. The glass capillaries were then pulled using a P-2000 micropipette puller *(Sutter Instruments, Novato, USA)*, dipped into 90°C epoxy for 30s *(Epo-Tek 301, Epoxy Technology, MASS, USA)* and cleaned in hot acetone for 3s. The electrodes were heated at 100°C for 12h and 150°C for 5 days. Electrodes were then polished and filed with potassium acetate at 4M and potassium chloride at 150 mM. The protruding carbon fibers were cut using a scalpel blade

under direct visualization to a length allowing to obtain maximal basal currents of 100 to 180 nA. The electrodes were calibrated with 1 µM DA in aCSF before and after each recorded slice and the mean of the current values obtained were used to determine the amount of released DA. After use, electrodes were cleaned with isopropyl alcohol *(Bioshop, France)*. The potential of the carbon fiber electrode was scanned at a rate of 300 V/s according to a 10 ms triangular voltage wave (−400 to 1000 mV vs Ag/AgCl) with a 100 ms sampling interval, using a CV 203BU headstage preamplifier *(Molecular Devices)* and a Axopatch 200B amplifier *(Molecular Devices, USA)*. Data were acquired using a Digidata 1440a analog to digital converter board *(Molecular Devices, USA)* connected to a computer using Clampex *(Molecular Devices, USA)*. Slices were left to stabilize for 20 min before any electrochemical recordings. After positioning of the bipolar stimulation electrode or the optical probe and carbon fiber electrodes in the tissue, single pulses (400 µA or 30 mW, 1ms,) or pulses-train (30 pulses at 10 Hz) were applied to the tissue to trigger DA release.

Behavioral analyses

Grip strength test. A grip strength apparatus *(BioSeb instruments, BIO-GS3, France)* was used to evaluate the paw force developed by Syt1 cKO^{DA} mice. 10-12-week-old male or female mice were held firmly by the tail and slowly lowered until their forepaws grasped the middle of the grid. Subjects were then lowered to a horizontal position and pulled following the axis of the sensor until they released their grasp on the grid. The maximum force exhibited by the subject was recorded. The test was repeated 3 times with 30 min resting period between each trial. The results are presented as the means of the 3 trials divided by the body weight of each recorded mouse.

Pole test. The test was conducted with a homemade 48-cm metal rod of 1-cm diameter covered with adhesive tape to facilitate traction, placed in a cage. 10-12-week-old male or

female Syt1 cKO^{DA} were positioned head-up at the top of the pole and the time required to turn (t-turn) and climb down completely was recorded. The results are presented as the mean of 2 sessions, with 3 trial per sessions for each mouse.

Rotarod. Motor coordination was evaluated with a rotarod apparatus *(Harvard Apparatus, LE8205, USA)*. 10-12-week-old male or female Syt1 cKO^{DA} mice were pre-trained on the rotarod for two consecutive days to reach a stable performance and then tested on day three. On the first day, mice were placed on the rotarod, rotating at a constant speed of 4 rpm. They remained on the rotarod until either one min had passed, or up to a maximum of 3 attempts at placing them on the rod. On the second day, mice were trained on the device with an accelerated rotation of 4 to 40 rpm, over a ten-min period. This training was repeated 3 times with approximately 30 min of rest between each trial. Mice were tested on the accelerating rod on day 3 and the latency to fall the device of each tested animal was recorded. The results are presented as the means of the 3 trials on day 3.

Open field. The locomotor behavior of 11-12-week-old male or female Syt1 cKO^{DA} mice was recorded using an infrared actimeter *(Superflex sensor version 4.6, Omnitech)* using the Fusion software *(v5.6 Superflex Edition).* A chamber partition was used to measure two mice at a time. Subjects were not given time to acclimate and spent a total of 60 min in the chamber with the following protocol: the first 20 min was used to record basal locomotion, while the following 40 min was used to record locomotion after saline or drug administration (i.p.). Drug treatments correspond to a single dose of cocaine hydrochloride at 20 mg/kg *(Medisca, cat# 53-21-4, Canada)* or D-amphetamine sulfate at 5 mg/kg *(Tocriss, 2813, UK)* at doses known to increase locomotion *(Itzhak and Martin, 1999; Steinkellner et al., 2014).* SCH23390-HCl *(Sigma, D-054, Canada) at* 50 µg/kg, quinpirole-HCl at 0.2 mg/kg *(Sigma, Q-102, Canada)* and raclopride L-tartrate at 1 mg/kg *(Sigma, R-121, Canada)* were also used at selected high doses known to reduce locomotion in the open field *(Centonze et al., 2003;*

Dourado et al., 2016; Radl et al., 2018). Each drug was diluted into 0.9% sodium chloride saline solution *(Halyard, #cat 116).* Results are presented as the mean of the traveled distance.

Autoradiography

10-12-week-old male or female Syt1 cKO^{DA} mice were anesthetized using pentobarbital NaCl solution (7 mg/mL) injected intraperitoneally and then were perfused intracardially with 20ml of PBS to remove the blood. The brains were extracted and quickly dipped in isopentane at -30°C for 1 min. 10-microns thick coronal sections of the whole striatum were then cut using a cryostat *(Leica Biosystem, Model 3050)* and mounted on charged microscope slides *(X-tra, Leica, Canada).* For binding assays, after a pre-wash step in Tris-HCl buffer (15 min) at room temperature, incubation was performed for 1h at room temperature in a 50 mM Tris-HCl buffer (pH 7.4), containing 120 mM NaC1, 5 mM KC1, 2 mM $CaC1_2$, 1 mM $MgC1_2$, in the presence of different concentrations (0.075 – 5 nM) of [^{3}H]-raclopride *(specific activity 82.8Ci/mmol, Perkin Elmer, #NET975250UC, Canada)* for D2 binding or different concentrations (0.150 – 10 nM) of [^{3}H]-SCH23390 *(specific activity 83.6Ci/mmol, Perkin Elmer, #NET930025UC, Canada)* for D1 binding. To determine the non-specific binding, adjacent sections were incubated respectively with 5 µM of sulpiride *(Sigma, cat#S7771, Canada)* for D2 binding and 20 nM mianserin hydrochloride *(Sigma, cat#M2525, Canada)* with 1 µM SCH-39166 hydrobromide *(Tocris, cat#2299, Canada)* for D1 binding. Incubation was terminated by rinsing sections twice for 5 min in ice-cold Tris-HC1, 50 mM (pH 7.4). Sections were then dipped briefly in cold distilled water and dried overnight. The microscope slides with tissue sections were placed in a light-proof X-ray cassette. Autoradiographs were prepared by placing the slide-mounted tissue sections in contact with a tritium-sensitive film *(Biomax MR, Kodack, cat#8715187, Canada)* for 6 weeks at room temperature. The films were then developed, and autoradiograms analyzed by densitometry. Autoradiograms were acquired using a grayscale digital camera *(Model CFW-1612M, Scion*

Corporation, Maryland, USA). The precise topography of D1 and D2 receptors in the striatum was determined from autoradiograms of 4 serial coronal sections for each dilution corresponding to approximately bregma +1.34 mm to 0.38 mm of the Paxinos and Watson mouse brain atlas *("Paxinos and Franklin's the Mouse Brain in Stereotaxic Coordinates, Compact - 5th Edition," 2019.)*. In each section, the caudate-putamen was arbitrarily divided into 4 quadrants (dorso-lateral, ventro-lateral, dorso-medial and ventro-medial). For each quadrant, the mean signal intensities were measured on ImageJ software and non-specific binding was subtracted from all density readings. The corrected optical gray densities of the different brain areas were converted into µCi/mg of tissue using a [^{3}H] radioactive standard disposed on each film *(American Radiolabeled Chemicals Inc., Cat# ART 0123A)*. The saturation binding curves were then analyzed on GraphPad software using a non-linear regression with the equation Y = Bmax*X/(Kd + X), where Y represents the specific binding values (µCi/mg of tissue) and X the radioligand concentration to estimate Bmax, the maximum specific binding and Kd, the radioligand concentration needed to achieve a half-maximum binding at equilibrium. The two last parameters were extracted and represent respectively the receptor density and the radioligands affinity for D1 or D2 receptors.

Tissue preparation and immunohistochemistry

10-12-week-old male or female Syt1 cKO^{DA} mice were anesthetized using a pentobarbital NaCl solution (7 mg/mL) injected intraperitoneally and then were perfused intracardially with 20 mL of PBS followed by 30 mL of paraformaldehyde (PFA) 4%. The brains were extracted, placed 48h in PFA followed by 48h in a 30% sucrose solution and frozen in isopentane at -30°C for 1 min. 40 microns thick coronal sections were then cut using a cryostat *(Leica CM1800)* and placed in antifreeze solution at -20°C until used. For slice immunostaining, after a PBS wash, the tissue was permeabilized, nonspecific binding sites were blocked and slices were incubated overnight with a rabbit anti-tyrosine hydroxylase (TH)

(1:1000, AB152, Millipore Sigma, USA), a rat anti-DAT *(1:2000, MAB369; MilliporeSigma, USA)*, a rabbit anti-VMAT2 *(1:2000, kindly provided by Dr. G.W. Miller, Emory University, USA (Cliburn et al., 2017))*, a rabbit anti-5-HT *(1:2000, 20080 ImmunoStar, In; USA)*, a chicken anti-GFP *(1:1000, GFP-1020; Aves Labs, USA)* and/or a rabbit anti-RFP *(1:1000, CA600-401-379, Rockland Inc., USA)* antibody. Primary antibodies were subsequently detected with rabbit, rat or chicken Alexa Fluor-488–conjugated, 546-conjugated and/or 647-conjugated secondary antibodies *(1:500, 2h incubation; Invitrogen, Canada)*. Slices were mounted on charged microscope slides *(Superfrost/Plus, Fisher Scientific, Canada)* and stored at 4°C prior to image acquisition.

Confocal imaging

Images were acquired using an Olympus Fluoview FV1000 point-scanning confocal microscope *(Olympus, Canada)* with a 60x oil-immersion objective (NA 1.42). Images acquired using 488nm, 546 nm and 647 laser excitations were scanned sequentially to prevent non-specific bleed-through signal. All image analysis was performed using ImageJ *(National Institutes of Health)* software. For the immunohistochemical characterization of brain tissue obtained from Syt1 cKO^{DA} mice or virally induced Syt1 KO mice, surface and intensity for each signal were measured in a series of 5 different striatal sections ranging from bregma +0.98 to bregma -1.06 mm, with a total of 22 different spots for each hemisphere (**Fig. S4A**).

Stereology

One out of every 6th cryostat section was used for TH immunostaining stereological counting of DA neurons. After a PBS wash, the tissue was incubated for 10 min with 0.9% H_2O_2 solution, then washed with PBS again and incubated for 48h with a rabbit anti-TH antibody *(1:1000, AB152, Millipore Sigma, USA)* at 4°C, 12h with goat anti-rabbit biotin-SP-AffiniPure secondary antibody *(111-065-003, Jackson ImmunoResearch Laboratories, USA)*

at 4°C and 3h with horseradish peroxidase streptavidin *(016-030-084, Cedarlane, USA)*. The diaminobenzidine (DAB) reaction was carried out for 45s, then stopped by incubation with 0.1M acetate buffer. Slices were mounted on charged microscope slides *(Superfrost/Plus, Fisher Scientific, Canada)* and left to dry for 96h after which they were stained with cresyl violet and went through incubations with increasing concentrations of alcohol. After short isopropanol and xylene baths, slides were sealed with Permount mounting medium *(SP15-100, Fisher, USA)* using glass coverslips. TH-immunoreactive neurons were counted in one out of every sixth section using a 100x oil-immersion objective on a Leica microscope equipped with a motorized stage. A 60 x 60 μm^2 counting frame was used in the Stereo Investigator *(MBF Bioscience)* sampling software with a 12 µm optical dissector (2 µm guard zones) and counting site intervals of 150 µm after a random start (100 µm intervals for unilateral lesion). Mesencephalic DA nuclei, including the VTA, SNc and RRF were examined. Stereological estimates of the total number of TH-immunoreactive neurons within each nucleus were obtained. The number of TH-negative neurons was also estimated similarly in each region based on cresyl violet staining.

Primary neuronal co-cultures

For all experiments, postnatal day 0-3 (P0-P3) mice were cryoanesthetized, decapited and used for co-cultures according to a previously described protocol *(Fasano et al., 2008)*. Primary DA neurons from VTA or SNc were prepared from $Syt1^{-/-}$ or $Syt1^{+/+}$ pups and co-cultured with ventral striatum and dorsal striatum neurons from $Syt1^{-/-}$ or $Syt1^{+/+}$ pups, respectively. Neurons were seeded (60 000 cells/mL) on a monolayer of cortical astrocytes grown on collagen/poly-L-lysine-coated glass coverslips. All cultures were incubated at 37°C in 5% CO_2 and maintained in 2/3 of Neurobasal, enriched with 1% penicillin/streptomycin, 1% Glutamax, 2% B-27 supplement and 5% fetal bovine serum *(Invitrogen, Canada)* plus 1/3 of minimum essential medium enriched with 1% penicillin/streptomycin, 1% Glutamax, 20mM

glucose, 1mM sodium pyruvate and 100 µl of MITO+ serum extender. All primary neuronal co-cultures were used at 14 days *in vitro* (DIV).

Immunocytochemistry on cell cultures

Cultures were fixed at 14-DIV with 4% paraformaldehyde (PFA; in PBS, pH-7.4), permeabilized with 0,1% triton X-100 during 20 min, and nonspecific binding sites were blocked with 10% bovine serum albumin during 10 min. Primary antibodies were: mouse anti-TH (*1:2000, MAB318, Millipore Sigma, USA*), rabbit anti-TH (*1:2000, AB152, Millipore Sigma, USA*), rabbit anti-Syt1 (*1:1000, 105-103, Synaptic Systems, Germany*), rabbit anti-VMAT2 (*1:2000, gift of Dr. Gary Miller, Colombia University*) and mouse anti-MAP2 (*1:2000, MAB3418, Millipore Sigma, USA*). These were subsequently detected using Alexa Fluor-488-conjugated, Alexa Fluor-546-conjugated, Alexa Fluor-568-conjugated and Alexa Fluor-647-conjugated secondary antibodies *(1:500, Invitrogen, Canada)*.

RT-qPCR

We used RT-qPCR to quantify the amount of mRNA encoding Syt1, 4, 7 and 11, Doc2b, TH, DAT and VMAT2 in brain tissue from P70 Syt1$^{+/+}$ and Syt1$^{-/-}$ mice. The brains were quickly harvested and the ventral mesencephalon containing SN/VTA structures were microdissected and homogenized in 500 µL of trizol. Next, RNA extraction was performed using RNAeasy Mini Kit *(Qiagen, Canada)* according to the manufacturer's instructions. RNA integrity was validated using a Bioanalyzer 2100 *(Agilent)*. Total RNA was treated with DNase and reverse transcribed using the Maxima First Strand cDNA synthesis kit with ds DNase *(Thermo Fisher Scientific)*. Gene expression was determined using assays designed with the Universal Probe Library from Roche *(www.universalprobelibrary.com)*. For each qPCR assay, a standard curve was performed to ensure that the efficiency of the assay was between 90% and 110%. Assay information is presented in **supplementary Table 1**. The QuantStudio qPCR

instrument *(Thermo Fisher Scientific)* was used to detect the amplification level. Relative expression comparison (RQ = 2^-ΔΔCT) was calculated using the Expression Suite software *(Thermo Fisher Scientific)*, using GAPDH as an endogenous control.

Western Blot

Striatum samples microdissected from $Sy1^{+/+}$, $Syt1^{+/-}$, $Syt1^{-/-}$ adult mice were lysed in RIPA buffer *(Fisher Scientific, PI89900)* containing a protease inhibitor cocktail *(Sigma).* Homogenized tissue samples were centrifuged at 12000g for 30 min at 4°C. Supernatant was collected and protein quantification was done with BCA reagent *(Thermo Scientific Pierce BCA Protein Assay Kit, PI23227).* 20 µg of each sample was separated on 8% SDS-PAGE followed by transfer onto a nitrocellulose membrane. Membrane blocking was done with 10% skimmed milk for 90 min at RT with gentle shaking. The membranes were incubated overnight at 4°C with gentle shaking with rat anti-DAT *(1:1000, MAB369; MilliporeSigma, USA)*, rabbit anti-TH *(1:1000, AB152, Millipore Sigma, USA)*, rabbit anti-VMAT2 *(1:5000, kindly provided by Dr. G.W. Miller, Emory University, USA (Cliburn et al., 2017))* and mouse anti-β-actin *(1:5000, A3854, Sigma-Aldrich, Canada)* primary antibodies. Membranes were washed 5 times with TBST buffer for 5 min each time. After this, appropriate secondary antibodies (1:5000) were added and the incubation was done at RT for 90 min with gentle shaking. Membranes were washed again with TBST buffer for 5 times X 5 min and developed using Clarity Western ECL substrate *(Bio-Rad, 1004384863).* Images were captured on a Luminescent Image Analyzer *(GE Healthcare)* using Image quant LAS 4000 software. Membranes were stripped and re-probed for β-actin as a loading control.

Microdialysis guide cannula implantation

10-12 weeks old male and female Syt1 cKO^{DA} mice were anesthetized with sodium isoflurane (2.5% isoflurane at 0.5 L/min oxygen flow), coupled with infiltration analgesia of

1.5 mg/kg lidocaine/bupivacaine 10 min prior to incision of the skull and stereotaxic implantation with a microdialysis guide cannula *(CMA 7, Harvard Apparatus)* into the left dorsal subdivision of the striatum (coordinates: 1.0 mm anterior of bregma, 2.0 mm lateral of bregma, and -3.3 mm below pia) and the right substantia nigra and ventral tegmental area (coordinates: -3.3 mm anterior of bregma, -0.8 mm lateral of bregma, and -3.4 mm below pia) following Paxinos coordinates *("Paxinos and Franklin's the Mouse Brain in Stereotaxic Coordinates, Compact - 5th Edition," 2019.)*. These guide cannulas were then used to insert the microdialysis probes *(6 kDa MW cut-off, CMA 7, Harvard Apparatus)* into the target sites. Guide cannulas were secured with acrylic dental cement and an anchor screw was threaded into the cranium. Buprenorphine (0.05 mg/kg, subcutaneously) was used for postoperative analgesia (once daily for 2 days). Animals were allowed 1-week (housed one per cage) to recover from cannula implantation before dialysis measurements of extracellular DA, 3,4-dihydroxyphenylacetic acid (DOPAC), norepinephrine (NE), and serotonin (5-HT) levels by microdialysis. A removeable obturator was inserted into the cannula to prevent cerebrospinal fluid seepage and infection.

Microdialysis

Microdialysis probes were calibrated in aCSF containing (in mM): NaCl (126), KCl (3), $NaHCO_3$ (26), NaH_2PO_4 (3), $MgCl_2$ (1.3), $CaCl_2$ (2.3), and L-ascorbic acid (0.2). *In vitro* probe recovery ranged from 4% to 30% at a flow rate of 1 µl/min. A computer-controlled microinfusion pump *(CMA)* was used to deliver perfusate to the probes, and the dialysate was collected from the outlet line. Probes were inserted into the indwelling guide cannulas of the anesthetized animals and perfused with aCSF (flow rate set at 1 µl/min). To minimize the influence of needle trauma on experimental outcomes, dialysates samples were collected during a typical 60 min equilibration period but were discarded and not analyzed. Three samples were then taken at 20 min intervals for 60 min. Each 10 µl dialysate sample was

collected in a fraction vial preloaded with 1 µl of 0.25 mol/l perchloric acid to prevent analyte degradation and immediately stored at 4 °C for subsequent analysis. Following microdialysis, mice received an intraperitoneal injection of ketamine/xylazine (120 mg/10 mg/kg) and were intracardially injected with cold saline, decapitated and the brains were harvested. After the microdialysis experiments, the striatum of each mouse was microdissected, and flash frozen in isopentane cooled to -35 °C on dry ice and stored at -80 °C prior to HPLC quantification.

High performance liquid chromatography

Extracellular DA, DOPAC, 5-HT and NE concentrations in the left dorsal subdivision of the striatum and the right substantia nigra (SNc) and ventral tegmental area (VTA) were determined with high-performance liquid chromatography (HPLC) using a Dionex pump *(ultimate 3000)* coupled with electrochemical detection (EC) *(Isingrini et al., 2017)*. Samples were run through a Luna C18 (2) 75 mm × 4.6 mm 3 µm analytical column at a flow rate of 1.5 ml/min and the electrochemical detector *(ESA CoulArray, model #5600A)* was set at a potential of -250 mV and +300 mV. The mobile phase consisted of 6% methanol, 0.341 mM 1-octanesulfoic acid sodium salt, 168.2 mM sodium acetate, 66.6 mM citric acid monohydrate, 0.025 mM ethylenediamine-tetra-acetic acid disodium and 0.71 mM triethylamine adjusted to pH 4.0–4.1 with acetic acid. Using ESA's CoulArray software, the position of the peaks for each metabolite was compared to an external standard solution containing 25 ng/ml DA, DOPAC, 5-HT, NE and 50 mM acetic acid prepared fresh daily from stock solutions and loaded with samples into a refrigerated (10 °C) Dionex RS autosampler *(ultimate 3000)*. Under these conditions, the retention time for DOPAC, NE, DA, and 5-HT was approximately 2.5 min, 1.1 min, 2.8 min, and 3.76 min respectively, with a total run time of 22 min/sample. Chromatographic peak analysis was accomplished by identification of unknown peaks in a sample matched according to retention times from known standards using Chromaleon software. The mean standard (n = 5) was used to quantify unknown peaks and to have the same

retention time on each run. The analytical curve, as determined with duplicate standard solutions of DOPAC, NE, DA and 5-HT in nanopure water, was in the range of 7 to 500 ng/ml (R^2 = 0.9963, 0.9971, 0.9899 or 0.9775, respectively). The analytical curve was constructed by plotting the area under the curve. For tissular measures, microdissected striatum were homogenized in a solution which contained 45 µl of 0.25 M perchlorate and 15 µl of 2,3-dihydroxybenzoic acid (100 mg/ml) which served as an internal standard. Following centrifugation at 10,000 rpm for 15 min at 4 °C, the supernatant was isolated to detect DA, DOPAC, NE and 5-HT using HPLC-EC as previously described. In parallel, pellets were reconstituted in 50 µl of 0.1 N NaOH and kept for protein quantification using a BCA protein assay kit *(Thermo Scientific Pierce BCA Protein Assay Kit, PI23227)*. All concentrations are expressed as ng/ml.

Statistical analysis

Data are presented as mean ± SEM. Statistical analyses were performed with Prism 9 software (GraphPad). The level of statistical significance was established at $p < 0.05$ in one or two-way ANOVAs with appropriate post-hoc tests or two-tailed t-tests with appropriate correction (*$p < 0.05$, **$p < 0.01$, ***$p < 0.001$, **** $p < 0.0001$).

Results

Syt1 is the main calcium sensor for fast axonal dopamine release.

In line with its high expression and localization in the axonal varicosities of DA neurons, Syt1 is a key regulator of activity-dependent DA release *(Mendez et al., 2011; Banerjee et al., 2020b; Ducrot et al., 2021)*. We generated conditional deletion of Syt1 in DA neurons (Syt1 cKO^{DA}), by crossing $Syt1^{lox/lox}$ mice with $DAT^{IREScre}$ mice **(Fig. 1A)**. Validating earlier results, we found using FSCV *ex vivo* in brain slices of $Syt1^{+/+}$, $Syt1^{+/-}$ and $Syt1^{-/-}$ mice an extensive reduction of phasic DA release induced by single electrical pulses in both the dorsal striatum (**Fig. 1B**: 0.074 µM ± 0.012 µM, n = 8 mice, vs 1.423 µM ± 0.15 in $Syt1^{+/+}$; n = 9 mice; 1-way ANOVA with Tukey, $p < 0.0001$) and ventral striatum (**Fig. 1C**: 0.144 µM ± 0.02 µM, n = 8 mice, vs 1.252 µM ± 0.08 in $Syt1^{+/+}$; n = 9 mice; 1-way ANOVA with Tukey, $p < 0.0001$) of $Syt1^{-/-}$ mice. In $Syt1^{-/-}$ mice, the residual signal was low in amplitude but still represented DA, as confirmed by the cyclic voltammogram (**Fig. S1A and 1B**). Stimulation with 10 Hz pulse trains only caused a very modest increase in DA overflow, only reaching significance in the ventral striatum (**Fig. S1D**). Mice in which DA neurons expressed a single allele of Syt1 also showed a small decrease in DA release, which reached significance in the ventral striatum (0.999 µM ± 0.03 µM, n = 8 $Syt^{+/-}$ mice; 1-way ANOVA with Tukey, $p < 0.0001$) (**Fig. 1C).** This observation argues for the existence of only a modest safety factor in the amounts of Syt1 required for normal function of DA neuron terminals. We conclude that Syt1 acts as the main calcium sensor for fast activity-dependent DA release in the striatum, but that other calcium sensors are also likely to play a complementary role, which may be more extensive in the ventral (nucleus accumbens) compared to dorsal striatum.

Syt1 deletion also reduces DA release in the ventral mesencephalon.

As DA release in cell body region of DA neurons is also calcium-dependent and since synaptotagmin isoforms and active zone proteins have been suggested to have a role in STD DA release *(Mendez et al., 2011; Robinson et al., 2019; Delignat-Lavaud et al., 2021)*, we also examined activity-dependent DA overflow in the ventral mesencephalon (**Fig. 1D**). We first measured DA release in the VTA of Syt1$^{-/-}$ mice using an optimal FSCV paradigm, with pulse-train stimulation (30 pulses at 10 Hz) and aCSF containing the DAT blocker nomifensine and the D2 antagonist sulpiride, allowing the detection of STD DA release without the influence of DA uptake and D2 autoreceptors activation *(Delignat-Lavaud et al., 2021)*. We observed a robust ≈68% decrease of activity-dependent DA overflow in Syt1$^{-/-}$ mice (0.09 µM ± 0.009 µM, n = 8, vs 0.277 µM ± 0.03 µM in n = 9 Syt1$^{+/+}$ mice; 1-way ANOVA with Tukey, $p < 0.0001$). This decrease was also significant in heterozygote mice (0.196 µM ± 0.02 µM, n = 8; 1-way ANOVA with Tukey, $p = 0.0310$). Similar recordings performed in the SNc also revealed a robust reduction (≈65%) of evoked DA overflow (**Fig. S1C** - 0.087 µM ± 0.01 µM, n = 5 Syt1$^{-/-}$ mice vs 0.25 ± 0.04 µM, n = 6 Syt1$^{+/+}$ mice; Welch's t-test, $p = 0.0103$).

Because there is yet no evidence for the presence of Syt1 in the STD compartment of DA neurons *(Mendez et al., 2011)* or any other neurons, this finding was unexpected. Interestingly, although the VTA region is well known for containing the cell body and dendrites of DA neurons, it has also been previously suggested to contain a small contingent of local dopaminergic axon collaterals with potential axonal release sites *(Rice and Patel, 2015)*. The available anatomical data is however limited *(Deutch et al., 1988; Bayer and Pickel, 1990)*. On the other hand, the SNc is believed to be devoid of axonal DA release sites *(Juraska et al., 1977; Wassef et al., 1981; Matsuda et al., 2009)*, but here again, the supporting data is limited.

Somatodendritic optogenetic stimulation reveal unaltered STD DA release in the absence of Syt1.

In view of the surprising reduction of evoked DA overflow in the ventral mesencephalon of Syt1$^{-/-}$ mice, we devised a new strategy to trigger STD DA release more selectively. For this, we combined FSCV with selective optogenetic stimulation of the STD compartment of neurons by expressing a STD-targeted version of channelrhodopsin (ChR2-Kv) (**Fig. 2**). Kv2.1 channels were previously reported to be restricted to the somatic and proximal dendritic membrane and absent from distal dendritic membrane, axons, and nerve terminals of cortical and hippocampal neurons *(Lim et al., 2000; Misonou et al., 2005; Jensen et al., 2017).* A 65 amino acid motif of the Kv2.1 voltage-gated potassium channel fused with the carboxy terminus of ChR2-EYFP *(Baker et al., 2016)* was inserted in a Cre-dependent AAV vector (AAV2/5-hsyn-DIO-ChR2-eYFP-Kv). A standard cell-wide hChR2 (AAV2/5-hsyn-DIO-ChR2-eYFP), previously used to trigger DA release in the striatum *(O'Neill et al., 2017)* and mesencephalon *(Delignat-Lavaud et al., 2021)* was used as a control.

Validation of the construct in primary DA neurons from DAT^{IRES}Cre mice showed the expected STD expression of the ChR2-Kv construct, with no expression in TH^{+}/MAP2^{-} processes and varicosities (**Fig. S2).** Expression of the construct *in vivo* in DAT^{IRES}Cre mice was efficient and restricted to the ventral mesencephalon (**Fig. 2A**). Confocal imaging at 60X revealed a membrane localization of ChR2-Kv at the soma of DA neurons (**Fig. 2B**). In the striatum, no eYFP signal was detected in the dorsal striatum but sparse signal was detectable in the ventral striatum, suggesting limited expression in a subset of VTA DA neuron axons in addition to the predominant STD expression. In line with this limited axonal expression of ChR2-Kv, DA release triggered by single-pulse optogenetic stimulation of ChR2-Kv in the striatum (dorsal and ventral) of Syt1$^{+/+}$ mice was more than 3-fold lower compared to release evoked with conventional ChR2 (0.3909 µM ± 0.05 µM, n = 7 mice vs 1.36 µM ± 0.2 µM, n = 7 mice; 2-way ANOVA with Tukey, $p < 0.0001$). Although evoked DA overflow in Syt1$^{-/-}$ mice was 2-fold lower compared to Syt1$^{+/+}$ mice, the difference did not reach statistical significance

most likely due to the small size of the responses and their heterogeneity (**Fig. 2C**) (0.21 µM ± 0.05 µM, n = 9 mice; 2-way ANOVA with Tukey, p = 0.3287). The sodium channel blocker TTX (1µM) abolished this small axonal DA release in all mice, thus demonstrating the requirement of action potentials in the response (**Fig. 2E**).

In the VTA (**Fig. 2D**), the release of DA induced by optogenetic train stimulation with hChR2 was easily detectable and of an amplitude similar to previously reported (203 nM ± 13 nM, n = 5 mice) *(Delignat-Lavaud et al., 2021)*. Release evoked by optogenetic stimulation with ChR2-Kv in Syt1$^{+/+}$ mice was significantly lower (132 nM ± 16 nM, n = 7 mice; 2-way ANOVA with Šidák, p <0.0001) compared to hChR2 (203 nM ± 13 nM, n = 5 mice) (**Fig. 2E**) and the signal detected in Syt1$^{-/-}$ mice was lower compared to Syt1$^{+/+}$ mice (57 nM ± 7 nM, n = 9 mice; 2-way ANOVA with Šidák, p <0.0001). To exclude any contribution from axonal DA release, additional FSCV recordings were obtained in the presence of TTX (1 µM). Under these conditions, STD DA release evoked by optogenetic stimulation of ChR2-Kv in Syt1$^{+/+}$ mice (44 nM ± 8 nM, n = 7 mice) was not significantly reduced compared to Syt1$^{-/-}$ mice (28 nM ± 7 nM, n = 9). Together these observations suggest that selectively triggered STD DA release is unaltered by loss of Syt1. The results also suggest that some of the DA release evoked by train stimulation in the ventral mesencephalon includes an axonal component, with electrical and optical stimulation with hChR2 therefore triggering a mixture of axonal and STD DA release.

Syt1 cKO^{DA} mice do not exhibit substantial motor defects.

DA is known to play a key role in multiple forms of movement *(Bergquist et al., 2003; Joshua et al., 2009)*. Notably, loss of striatal DA innervation in PD is responsible for the cardinal motor features observed in the disease *(Halliday et al., 1990)*. Blockade of DA receptors induces catalepsy and a range of other motor deficits in rodents and other species

(Hauber, 1996; Ward and Citrome, 2018). Based on our results showing a dramatic impairment of phasic DA release in Syt1$^{-/-}$ mice, we hypothesized that this would lead to major motor deficits in Syt1 cKO^{DA} mice.

First, we evaluated motor coordination using the rotarod (**Fig. 3A**) and the pole test (**Fig. 3B**). Surprisingly, Syt1$^{-/-}$ and Syt1$^{+/-}$ showed no deficits and even exhibited better performance on the rotarod task than wild type littermates, with a significantly higher latency to fall from the rod (124s ± 12 for Syt1$^{+/+}$ mice vs 197s ± 23s for Syt1$^{+/-}$ mice; p = 0.0220 and 188s ± 20s for Syt1$^{-/-}$ mice; 1-way ANOVA with Dunnett test, p = 0.0460 vs; n = 8 mice). In the pole test, no statistical difference was observed between genotypes for the time required for the animals to orient themselves facing in a downward direction (t-turn). For the time required to climb-down the pole, no difference was detected between Syt1$^{+/+}$ and Syt1$^{-/-}$ mice, although Syt1$^{+/-}$ mice performed the task faster than WT mice (8s ± 0.7s vs 11s ± 0.5s for Syt1$^{+/+}$, n = 8; 1-way ANOVA with Dunnett test, p = 0.0414). Front paw grip strength was evaluated in the grip test (**Fig. 3C**). No statistical differences were observed regarding the force developed by the mice on the grid.

We next measured spontaneous locomotion and locomotion induced by the psychostimulant drugs cocaine (20 mg/kg) and amphetamine (5 mg/kg). We measured the traveled distances using an open field for 20 min, followed by another 40 min after drug or vehicle injection (0.9% saline). No difference was detected between Syt1$^{+/+}$ and Syt1$^{-/-}$ mice on basal locomotion after saline injection (**Fig. 3D**), with only a non-significant trend for higher traveled distance within the 5 min post injection in Syt1$^{+/-}$ mice (**Fig. 3L**, 91% of baseline ± 16% vs 56% ± 13% for Syt1$^{+/+}$ mice, n = 8; 1-way ANOVA with Dunnett test, p = 0.1211).

The increased locomotor response to the DA transporter blocker cocaine was comparable between genotypes (**Fig. 3E and G).** However, locomotion induced by the DA

releaser amphetamine was sharply elevated in Syt1$^{-/-}$ mice 10 min after the injection (+714% ± 103% vs +252 ± 29% in Syt1$^{+/+}$, n = 8; 1-way ANOVA with Dunnett test, p = 0.0046), which became maximal 20 min post-injection (+1045% ± 126% vs 523 ± 58%, n = 8; 1-way ANOVA with Dunnett test, p = 0.0069) (**Fig. 3F)**. Cumulative distance for the 40 min under treatment confirmed this effect with an average traveled distance for Syt1$^{-/-}$ mice of +777% ± 67% vs 472% ± 53% for Syt1$^{+/+}$ (2-way ANOVA with Tukey, p = 0.0004) and +481% ± 73% for Syt1$^{+/-}$ mice (2-way ANOVA with Tukey, p = 0.0009) **(Fig. 3G**).

The observed increase in amphetamine-induced locomotion could result from increased amphetamine-induced DA secretion or from postsynaptic DA receptor sensitization. We next tested this hypothesis by administering the selective D1 receptor agonist SCH23390 (50 µg/kg), the D2 receptor agonist quinpirole (0.2 mg/kg) or the D2 receptor antagonist raclopride (1 mg/kg). At the selected doses, all drugs caused an abrupt decrease in locomotion, with no significant differences between genotypes when considering the complete drug treatment period (**Fig. 3H-J-K**). However, when we compared the mean traveled distance within the first 5 min following drug injection (**Fig. 3L**), Syt1$^{-/-}$ mice showed a lower traveled distance in response to the D2 agonist quinpirole compared to Syt1$^{+/+}$ mice (respectively 21% ± 3% n = 10, vs 47% ± 8%, n = 8; 1-way ANOVA with Dunnett test, p = 0.0044). The opposite pattern was detected in response to the D2 antagonist raclopride, with a significantly increased response in the Syt1$^{-/-}$ mice compared to Syt1$^{+/+}$ mice (14% ± 3% in Syt1$^{-/-}$ vs 3% ± 1% in Syt1$^{+/+}$, n = 10; 1-way ANOVA with Dunnett test, p = 0.0056). During this period, no significant differences were once again observed among genotypes after the injection of the D1 agonist SCH23390.

Taken together, these results suggest that despite a >90% impairment of phasic DA release in the striatum and a substantial decrease in DA release in the mesencephalon, Syt1 cKO^{DA} mice do not exhibit any obvious defects in basic unconditioned DA-dependent motor

tasks. Our observations lead us to hypothesise that such behaviors do not require phasic, activity-dependent DA release and can be maintained by basic resting levels of extracellular DA. Our results with D2 receptor ligands further suggest that adaptations are likely to occur in the DA system in these mice, in a manner that is similar to adaptations occurring at early stages of DA neuron degeneration in PD. In particular, D2 receptors can be hypothesized to undergo an increased density and/or affinity.

Increased D2 autoreceptor and DAT function in Syt1 cKO^{DA} mice

As a first step to examine underlying adaptations to the DA system in Syt1 cKO^{DA} mice, we used FSCV to probe the functionality of D2 autoreceptors and of the membrane DA transporter (DAT) in the dorsal and ventral striatum. We measured the impact on DA release of the D2 receptor agonist quinpirole (1 µM). In line with previous work showing that D2 autoreceptors negatively regulated DA release *(Stamford et al., 1988; Palij et al., 1990)*, DA overflow evoked by single pulses was decreased by ≈85% in the dorsal striatum (1.38 µM ± 0.18 µM pre-treatment vs 0.21 µM ± 0.07 µM after treatment, n = 9; Welch's t-test, p = 0.0001) and by ≈84% in the ventral striatum (1.22 µM ± 0.1 µM pre-treatment vs 0.196 µM ± 0.06 µM after treatment, n = 9; unpaired t-test, p < 0.0001) after a 15 min perfusion of quinpirole (**Fig. 4A, 4B**). In Syt1$^{-/-}$ mice, quinpirole caused a complete abolition of detectable DA release in both the dorsal striatum (0.061 µM ± 0.006 µM) and ventral striatum (0.004 µM ± 0.002 µM pre-treatment vs 0.13 µM ± 0.02 µM after treatment, n = 8; Welch's t-test, p = 0.0014). This observation further confirms that the remaining signal detected by FSCV in Syt1$^{-/-}$ mice is indeed DA. The increased relative effect of D2 autoreceptor stimulation **(Fig. 3**) also supports the hypothesis of an increased sensitivity of D2 receptors in Syt1$^{-/-}$ mice.

We next evaluated the impact of the D2 autoreceptor antagonist sulpiride, previously shown to enhance DA release triggered by pulse trains *(Fawaz et al., 2009)*. DA release evoked

by pulse trains (30 pulses at 10 Hz) in the striatum of Syt1$^{+/+}$ mice was robustly increased by sulpiride (5 µM) in both the dorsal striatum (149%) (1.34 µM ± 0.1 µM pre-treatment vs 2.0 µM ± 0.19 µM after treatment, n = 8; unpaired t-test, p = 0.0079) and ventral striatum (167%) (1.13 µM ± 0.08 µM pre-treatment vs 1.89 µM ± 0.21 µM after treatment, n = 8; Welch's t-test, p = 0.0085) (**Fig. 4C, 4D**). Despite a dramatic impairment of DA release evoked by train stimulation in Syt1$^{-/-}$ mice (**Fig. S1D**), the relative effect of sulpiride on evoked DA release was similar in magnitude compared to the wild type animals in the dorsal striatum, with a +140% increase (0.068 µM ± 0.007 µM pre-treatment vs 0.095 µM ± 0.01 µM after treatment, n = 11; unpaired t-test, p = 0.0466). In the ventral striatum, the relative effect of sulpiride on train-evoked DA overflow was higher in Syt1$^{-/-}$ compared to Syt1$^{+/+}$ mice, with a +261% increase (0.13 µM ± 0.02 µM pre-treatment vs 0.34 µM ± 0.08 µM after treatment, n = 11; Welch's t-test, p = 0.0318). Together with our results with quinpirole, these findings again argue that D2 autoreceptor function is increased in Syt1$^{-/-}$ mice, especially in the ventral striatum region.

Finally, we evaluated the functionality of the DAT by quantifying the impact of the DAT blocker nomifensine (5 µM) on train-evoked DA overflow. As expected, such treatment greatly enhanced DA overflow in wild type animals, with a +288% increase in the dorsal striatum (1.79 µM ± 0.19 µM pre-treatment vs 5.15 µM ± 0.74 µM after treatment, n = 4; unpaired t-test, p = 0.0045) and a +221% increase in the ventral striatum (1.51 µM ± 0.2 µM pre-treatment vs 3.34 µM ± 0.52 µM after treatment, n = 4; unpaired t-test, p = 0.0173) (**Fig. 4E, 4F**). The relative effect of nomifensine in Syt1$^{-/-}$ mice was significantly higher than in Syt1$^{+/+}$ mice, with a +685% increase in the dorsal striatum (0.108 µM ± 0.03 µM pre-treatment vs 0.74 µM ± 0.22 µM after treatment, n = 6; Welch's t-test, p = 0.0367) and a +544% in the ventral striatum (0.16 µM ± 0.03 µM pre-treatment vs 0.87 µM ± 0.13 µM after treatment, n = 6; Welch's t-test, p = 0.0162) (**Fig. 4E, 4F**). These results demonstrate that DAT function is

intact in Syt1$^{-/-}$ mice. Interestingly, they further suggest that nomifensine may act in some way to rescue part of the impaired activity-dependent DA release in these mice. Although speculative, this could be through its electrogenic activity that directly modulates membrane potential *(Carvelli et al., 2004).*

Higher D2 receptor density with no change in affinity in Syt1 cKO^{DA} mice

As the maintenance of motor behaviors in Syt1$^{-/-}$ mice could be due in part to adaptations of presynaptic and/or postsynaptic DA receptors in the striatum, we next used autoradiography to quantify D1 and D2 binding using the selective D1 and D2 receptor radioligands [^{3}H]-SCH23390 and [^{3}H]-raclopride, respectively. No change of Kd for D1 or D2 binding was observed in any analyzed striatal region (dorso-lateral, ventro-lateral, dorso-medial and ventro-medial), indicating that receptor affinity for these radioligands was unchanged in Syt1 cKO^{DA} mice (**Fig. S3**). Similarly, no change of maximal binding capacity (Bmax) was observed for the D1 receptor (**Fig. 5A**). However, a significant increase in D2 receptor Bmax was detected in the ventro-lateral part of the striatum of Syt1$^{-/-}$ mice (**Fig. 5B**, 81.7 µCi/mg of tissue ± 14.5 vs 46.3 µCi/mg ± 4.2, n = 4 mice; unpaired t-test, p = 0.0413). A tendency for a general increase of Bmax in the whole striatum was also observed (57.3 µci/mg ± 9 vs 36.7 µCi/mg ± 4.1, n = 4 mice; unpaired t-test, p = 0.0697). The lack of change in D1 receptor binding in Syt1 cKO^{DA} mice is in line with the lack of change in the behavioral response to the D1 receptor antagonist SCH23390 in Syt1$^{-/-}$ mice. The increased D2 receptor binding observed in the ventro-lateral striatum of these mice is compatible with our observation of increased behavioral responses to the D2 receptor antagonist raclopride. It also provides further support for the hypothesis that in the absence of evoked DA release, adaptations to DA receptors combined with maintained basal extracellular DA levels are sufficient to support many types of unconditioned DA-dependent behaviors.

Adaptations of DA synthesis and packaging in Syt1 cKO^{DA} mice

Compensatory changes at early stages of DA neuron degeneration in PD include not only receptor adaptations, but also enhanced DA synthesis *(Donnan et al., 1991; Richard and Bennett, 1994)* and increased axonal sprouting. The later has been linked to reduced activation of D2 autoreceptors *(Parish et al., 2001; Tripanichkul et al., 2003; Fasano et al., 2008; Fasano et al., 2010, 2013; Giguère et al., 2019).* We therefore hypothesized that reduced activity-dependent DA release in Syt1$^{-/-}$ mice might lead to an increased density of DA neuron terminal markers in the striatum. We next used immunohistochemistry and quantitative confocal microscopy to measure striatal levels of the DA synthesis enzyme TH, the vesicular DA transporter VMAT2 and the DAT. Serotonin (5-HT) innervation was also examined because previous work showed that this system undergoes compensatory sprouting in response to reduced DA levels *(Gagnon et al., 2018).*

We measured signal surface and intensity for these markers in a series of 5 different striatal slices ranging from bregma +0.98 to bregma -1.06 mm, with a total of 22 different areas for each hemisphere (**Fig. S4A**). We found a global increase of TH signal surface in Syt1$^{-/-}$ mice compared to Syt1$^{+/+}$ animals, both in the dorsal striatum (135% ± 6% of control n = 20 hemispheres from 10 mice; 2-way ANOVA with Šidák, p = 0.0001) and ventral striatum (148% ± 6% of control, n = 20/10 mice; 2-way ANOVA with Šidák, p <0.0001) (**Fig. 6A, 6B**). A global increase of TH signal intensity was also observed, in the dorsal (117% ± 3% of control, n = 20/10 mice; 2-way ANOVA with Šidák, p = 0.0005) and ventral striatum (125% ± 4% of control, n = 20/10 mice; 2-way ANOVA with Šidák, p <0.0001) (**Fig. 6C**). A similar increase in the surface of VMAT2 immunoreactivity (145% ± 10% of control, n = 20/10 mice; 2-way ANOVA with Šidák, p = 0.0043) and in the intensity of VMAT2 signal (123% ± 5% of control, n = 20/10 mice; 2-way ANOVA with Šidák, p = 0.0011) was observed in the dorsal striatum and in the ventral striatum (signal surface; 157 ± 10% of control, n = 20/10 mice; 2-way

ANOVA with Šidák, p = 0.0003, signal intensity; 130% ± 5% of control, n = 20/10 mice; 2-way ANOVA with Šidák, p <0.0001). Overall, these results suggest that in Syt1$^{-/-}$ mice, the total density of dopaminergic axonal processes and possibly the total vesicular pool/stock of DA are increased, possibly explaining the selective increase in amphetamine-induced but not cocaine-induced locomotion in these mice.

Opposite changes in striatal DAT immunostaining were observed in Syt1 cKO^{DA} mice, with a global decrease of signal surface in the dorsal striatum (62% ± 6% of control, n = 20/10 Syt1$^{-/-}$ and 22/11 Syt1$^{+/+}$; 2-way ANOVA with Šidák, p =0.0094) and in the ventral striatum (64% ± 7% of control, n = 20/10 Syt1$^{-/-}$ and 22/11 Syt1$^{+/+}$; 2-way ANOVA with Šidák, p =0.0131) (**Fig. 6A, B, C**). The DAT signal intensity appeared unchanged in the ventral striatum but was significantly decreased in the dorsal striatum (89% ± 2% of control, n = 20/10 Syt1$^{-/-}$ and 22/11 Syt1$^{+/+}$; 2-way ANOVA with Šidák, p = 0.0280).

These results are compatible with the establishment of compensatory mechanisms acting together to maintain extracellular DA levels in the striatum Syt1 cKO^{DA} mice. These compensatory changes in TH and VMAT2 occurred in the absence of any change in DA neuron number in the VTA and SNc of Syt1$^{-/-}$ mice, as confirmed by stereological counting of TH-positive neurons in these structures (**Fig. 6D**).

Finally, while 5-HT immunoreactive signal intensity in the striatum remained unchanged after Syt1 deletion, a small decrease of the 5-HT signal surface was visible in the dorsal striatum (72% ± 8 of control, n = 20/10 Syt1$^{-/-}$ and 22/11 Syt1$^{+/+}$; 2-way ANOVA with Šidák, p = 0.0399) and ventral striatum (65% ± 7 of control, n = 20/10 Syt1$^{-/-}$ and 22/11 Syt1$^{+/+}$; 2-way ANOVA with Šidák, p = 0.0114) (**Fig. 6A, B, C**). This result demonstrates a lack of serotoninergic compensatory sprouting in the striatum of Syt1 cKO^{DA} mice.

Arguing that compensatory adaptations occur gradually in Syt1$^{-/-}$ mice during the postnatal period as a result of abrogation of activity-dependent DA release, we observed no significant changes in the general morphological development of DA neurons isolated from P0-P3 pups and grown *in vitro* for 2-weeks (**Fig. S5**).

Primary postnatal mesencephalic DA neurons from Syt1$^{-/-}$ mice were examined to identify any developmental changes resulting from loss of Syt1. As expected, Syt1 immunoreactivity was absent from the axonal varicosities of these neurons (**Fig. S5A)** (n = 29 fields for Syt1$^{-/-}$ and 35 for Syt1$^{+/+}$). A subset of these TH-positive axonal varicosities was also positive for VMAT2, a proportion that was not different in Syt1$^{-/-}$ mice compared to Syt1$^{+/+}$ mice (**Fig. S5B and G,** n = 50 fields for Syt1$^{-/-}$ and 55 for Syt1$^{+/+}$). Most of these varicosities were non-synaptic in structure, as revealed by the observation that only a very small subset was in contact with a MAP2-positive dendritic segment independently of mouse genotype (**Fig. S5C and F**, n = 47 fields for Syt1$^{-/-}$ and 64 for Syt1$^{+/+}$), in line with recent results *(Ducrot et al., 2021)*. The intensity of TH immunoreactivity in the axon terminals and of VMAT2 in the cell body of DA neurons was also unchanged in Syt1$^{-/-}$ mice compared to Syt1$^{+/+}$ mice (**Fig. S5H, J)** (TH; n = 138 fields for Syt1$^{-/-}$ and 166 fields for Syt1$^{+/+}$, VMAT2; n = 17 Syt1$^{-/-}$ fields and 22 Syt1$^{+/+}$ fields). A small increase in VMAT2 signal in the axon terminals of Syt1$^{-/-}$ was however observed, similar to *in vivo* observations (6002 ± 732 pixels/field, n = 43 for Syt1$^{-/-}$ fields vs 3765 ± 590 pixels/field, n= 45 for Syt1$^{+/+}$ fields; unpaired t-test p = 0.0191).

Survival of DA neurons in these cultures over 14 days was not significantly different between genotypes (**Fig. S5K**, n = 10 coverslips Syt1$^{+/+}$ and 12 Syt1$^{-/-}$). Finally, the number of axonal branches and their length was unchanged (**Fig. S5L, M, N, O**). These results argue that, *in vitro*, the basic development of DA neurons is not impacted by Syt1 deletion.

Finally, we also unveiled compensatory adaptations in adult Syt1 cKO^{DA} mice by quantification of mRNA levels in total microdissected ventral mesencephalon (**Fig. S6A**, n = 5 mice from each genotype). We observed significant upregulations (1-way ANOVA with Dunnett) of *th* (1.48 folds, p = 0.0142), *Slc6a3* (DAT) (1.38 folds, p =0.0339) and *Syt4* (1.25 folds, p = 0.0199) in Syt1$^{+/-}$ mice and upregulations of *Syt4* (1.29 folds, p = 0.0103) and *Syt7* (1.22 folds, p = 0.0474) in Syt1$^{-/-}$ mice. It should be noted that these changes of expression could be underestimated as our analysis was performed on whole microdissected ventral midbrains, therefore including non-dopaminergic neurons. This dilution effect is visible for instance in the Syt1 mRNA quantification, which is only reduced by ≈25% in Syt1$^{+/-}$ mice (p = 0.0065) and by ≈58% in Syt1$^{-/-}$ mice (p <0.0001). Adaptations also occurred at protein levels, as measured by Western Blot in total microdissected striatum (**Fig. S6B-F**), with a significant increase of the VMAT2 in Syt1$^{+/-}$ mice (1.2 fold; 1-Way ANOVA with Dunnett, p = 0.0270) and in Syt1$^{-/-}$ mice (1.38, p <0.0001). No change in relative protein levels was observed for TH and DAT.

Acute deletion of Syt1 in adult mice impairs DA release but prevents adaptations.

Since Syt1 cKO^{DA} developed strong adaptations, which likely happened during postnatal development, we knocked out Syt1 in adult mice by injecting 6-7 weeks old Syt1$^{lox/lox}$ mice with an AAV vector allowing expression of the Cre recombinase in DA neurons (AAV9-TH-cre-myc-2A-fusion-red). Three weeks after stereotaxic virus injection in the mesencephalon of these mice, strong expression of the fusion-red reporter was detected in a majority of DA neurons (**Fig. 7A**). The reporter was also found in a subset of TH-negative neurons at the sites of infection, revealing the preferential but imperfect selectivity of the construct used. FSCV recordings in the striatum and mesencephalon of these mice revealed a robust decrease of DA release evoked by single electrical pulses compared to controls, both in the dorsal (0.44 µM ± 0.04 µM, n = 16/8 vs 1.12 µM ±0.07 µM, n = 14/7; 2-way ANOVA with

Šidák, p <0.0001) and ventral striatum (0.37 µM ± 0.03 µM n = 16/8 vs 0.89 µM ± 0.1 µM, n = 14/7; 2-way ANOVA with Šidák, p <0.0001). DA release in the VTA of Cre virus injected mice showed a strong decrease in comparison to control mice injected with the control AAV (CTRL; 0.24 µM ± 0.03 µM, n = 14/7, Cre AAV; 0.026 µM ± 0.01 µM, n = 16/8; 2-way ANOVA with Šidák, p = 0.0171). This result validates the key role of Syt1 as the main calcium sensor controlling phasic DA release in the adult brain.

Immunohistochemical analysis of TH and DAT in these Syt1 adult KO mice showed that both TH and DAT surface and signal intensity were unchanged, except for a slight increase of the TH signal surface in the ventral striatum (n = 12 hemispheres/6 mice) (+139% ± 18% vs control; 2-way ANOVA with Šidák, p =0.0348) (**Fig. 7C, D, E**). Overall, these results reveal that adult deletion of Syt1 leads to a strong reduction of activity-dependent DA release, accompanied by blunted neuroanatomical adaptations in comparison with conditional Syt1 cKO^{DA} mice.

Basal extracellular DA levels and total tissue DA are not altered in Syt1 cKO^{DA} mice

Based on our FSCV and anatomical results showing a range of adaptations similar to those occurring at early stages of PD and potentially enhancing the response to basal extracellular DA, we hypothesize that DA-dependent motor behaviors in Syt1 cKO^{DA} mice are maintained because of the presence of sufficient basal levels of extracellular DA in the striatum of these mice. To test this hypothesis, we used microdialysis in anesthetized mice implanted with two cannulas to measure extracellular DA and metabolites in the dorsal striatum and in the ventral mesencephalon. Following this sampling, the striatum of each animal was also microdissected and the total striatal content of DA and metabolites were quantified by HPLC (**Fig. 8A**). Our results reveal that striatal tissue contents of DA, DOPAC, serotonin (5-HT) and norepinephrine (NE) were not significantly different in $Syt1^{-/-}$ mice (n = 12) compared to

Syt1$^{+/+}$ mice (n = 10) and (**Fig. 8B**). In addition, the DA/DOPAC ratio was found to be unchanged in Syt1$^{-/-}$ mice, suggesting an intact DA turnover. Microdialysis similarly revealed that even if activity-dependent DA release was mostly blocked in Syt1$^{-/-}$ mice, basal extracellular DA levels in the striatum and mesencephalon of these mice were not reduced in comparison to Syt1$^{+/+}$ mice (**Fig. 8C**). Similarly, extracellular levels of DOPAC, 5-HT and NE were unchanged. Together, these results indicate that the pool of releasable DA is not decreased by loss of Syt1 and that these mice can maintain intact and sufficient levels of extracellular DA to maintain a basal tone of D1 and D2 receptor activation.

Discussion

In the present study, we find that Syt1 is the main calcium sensor involved in fast activity-dependent DA release, confirming previous results obtained first *in vitro (Mendez et al., 2011),* and more recently *in vivo (Banerjee et al., 2020b).* Our work confirms, but also extends, these previous observations in three ways.

First, while previous *in vivo* work using amperometry concluded that release evoked by single spikes was completely abrogated in Syt1$^{-/-}$ mice, we find that a small component of evoked DA release is in fact maintained in the dorsal (≈5%) and ventral striatum (≈12%) This remaining release was abolished using the D2 receptor agonist quinpirole. This observation, together with the analysis of voltammograms, confirms the dopaminergic origin of the signal detected by FSCV in Syt1$^{-/-}$ mice and strongly suggests the involvement of another calcium sensor mediating fast, activity-dependent release. Syt7 would be a logical candidate because it was previously demonstrated to be highly expressed in DA neurons and localized in both axonal varicosities and in the somatodendritic compartment of these neurons *(Mendez et al., 2011).* Interestingly, we detected a small increase in Syt7 mRNA purified from the ventral mesencephalon of Syt1$^{-/-}$ mice, suggesting a possible functional compensation by this calcium

sensor after Syt1 deletion **(Fig. S4)**. This modest 1.2-fold increase is likely to represent an underestimation of the real compensation because our analysis was performed on mRNA obtained from whole microdissected ventral mesencephalon, therefore including non-DA neurons. This situation also explains why Syt1 mRNA was only decreased by ≈58% in Syt1$^{-/-}$ mice. However, Syt7 constitutive KO mice were recently found to have no impairment of single-pulse evoked DA release in the striatum, instead playing a role in STD DA release *(Delignat-Lavaud et al., 2021)*. This absence of effect at the terminals echoes previous results in GABAergic neurons where Syt7 deletion failed to reduce fast synchronous release, slow asynchronous release, or short-term synaptic plasticity *(Maximov et al., 2008)*. However, a role of Syt7 in asynchronous release of neurotransmitter was demonstrated using double knock-out of Syt1 and Syt7 *(Bacaj et al., 2015, 2013)*. We can thus speculate that a role of Syt7 in gating evoked DA release would be unveiled by a double KO of Syt1 and 7 in DA neurons. Other synaptotagmin isoforms expressed in DA neurons could also be involved in supporting release in the absence of Syt1. We found that Syt4 mRNA is also upregulated in Syt1$^{-/-}$ mice. However, this isoform appears to only play a role in STD DA release in DA neurons *(Mendez et al., 2011; Delignat-Lavaud et al., 2021)*. Syt11, suggested to participate in regulating DA vesicle pool replenishment *(Wang et al., 2018)*, could also potentially be involved. Calcium sensors of the Doc2 family are also potential candidates because they have previously been shown to act as modulators of spontaneous synaptic transmission by a calcium-independent mechanism in cortical synapses *(Pang et al., 2011)*. However, expression of Syt11 and Doc2b were found to be unchanged in our RT-qPCR analysis of Syt1 cKO^{DA} mice.

Secondly, results from the current study extend previous work by showing that basal unconditioned motor functions in mice are unimpaired under conditions where most activity-dependent DA release from VTA and SNc DA neurons is blocked. This observation may be surprising considering that axonal and STD DA release is known to play a critical role in motor

control *(Bergquist et al., 2003; Joshua et al., 2009)*. Our work suggests that basal levels of DA in the striatum, deriving either from spontaneous exocytosis and/or from the very small remaining phasic or desynchronized release, are sufficient to support these basic behaviors and that a large phasic DA signal is not necessary.

Moreover, we find that Syt1 cKO^{DA} mice, despite a dramatic impairment of evoked DA release, produce viable, fertile offspring's, with normal body weight (data not shown) and no gross physical or behavioral abnormalities. However, we observed multiple behavioral, physiological and anatomical phenotypes pointing towards the establishment of functional adaptations that tune the DA system to the existing conditions by maximizing DA production and packaging as well as postsynaptic receptor activation.

In open-field experiments, we found that while cocaine-induced locomotion was unchanged in Syt1$^{-/-}$ animals, amphetamine-induced locomotion was robustly enhanced. Cocaine is known to increase extracellular DA by blocking reuptake through the DAT, while amphetamine induces a similar elevation by a more complex mechanism including impaired VMAT2-dependent vesicular storage and reverse transport *(Sulzer et al., 2005)*. These results, together with our observation of unchanged tissue DA levels, indicate that while the total pools of DA are not altered in Syt1 KO animals, there are pre- and postsynaptic adaptations taking place after the loss of Syt1. The observed increase in VMAT2 expression in Syt1 KO mice might explain in part the differential impact of loss of Syt1 on amphetamine and cocaine-induced locomotor activation. Our behavioral results with DA receptor agonists and our autoradiography results suggest that D2 receptors are most affected, with an increased response to the D2 agonist quinpirole and a reduced response to the D2 antagonist raclopride, together with increased D2 receptor binding in the ventro-lateral striatum. The D1 receptor system was unchanged in Syt1$^{-/-}$ animals, as no differences emerged for locomotion induced by the D1 agonist SCH23390, or for D1 ligand binding.

We also find clear presynaptic adaptations illustrated by an increase of TH and VMAT2 signal surface and intensity and a decrease in DAT immunoreactivity in both the ventral and dorsal striatum. One interpretation of the increases in TH and VMAT2 signal is that there may be an increase in the axonal arborization of DA neurons in Syt1$^{-/-}$ mice as well as a decrease in reuptake capacity. We and others have previously provided strong support for the hypothesis that DA, through D2 autoreceptors is a key regulator of axon growth by DA neurons *(Parish et al., 2002; Tripanichkul et al., 2003; Giguère et al., 2019)*. In the context of a strong reduction in evoked DA release, it is to be expected that D2 autoreceptors would be chronically under-stimulated leading to removal of a brake on axon growth and thus an enhanced density of terminals, in line with our recent work showing axonal arbor expansion after conditional deletion of the D2 receptor gene in DA neurons *(Giguère et al., 2019)*. Further experiments will be required to demonstrate such an axonal arbor expansion more directly in Syt1$^{-/-}$ mice. The decrease in DAT immunoreactivity suggests reduced expression of DAT in the KO mice. Our qPCR results show no change in DAT mRNA levels in the KO mice. Western blot also failed to detect a change in DAT protein, although an increase in VMAT2 levels was confirmed with this technique. Although speculative, it is possible that different pools of DAT are detected in fixed and non-fixed material. A reduced level of DAT on DA neuron axon terminals could in theory lead to reduced rates of DA reuptake and thus contribute to maintaining extracellular DA levels in the Syt1 deficient mice. Our FSCV experiments were not able to resolve this as the very small responses remaining in the KO mice precluded a reliable analysis of estimated reuptake kinetics. Quantifications of DAT function in striatal synaptosome preparations might help to resolve this.

Arguing that such compensatory changes in Syt1$^{-/-}$ mice result from an early and substantial loss of evoked DA release, we found little if any changes in TH and DAT immunoreactivity in adult mice in which Syt1 was deleted by injecting a TH-Cre virus in the

ventral mesencephalon. These results indicate that compensatory events are likely to take place during early pre- and postnatal development of the Syt1 KO mice. Another possibility is that the level of infection and impairment of DA release in the adult KO animals did not exceed the threshold necessary to induce compensatory mechanisms. Our *in vitro* results however suggest that lack of Syt1 does not lead to substantial alterations of the survival, growth and basic connectivity of DA neurons, further pointing towards the implication of circuit-level changes as drivers of the pre- and postsynaptic adaptations.

A third notable discovery deriving from the present work is the unexpected impairment of activity-dependent DA release in the ventral mesencephalon. This observation is surprising because on the one hand, DA release in this region is thought to derive mostly from the STD compartment of DA neurons, and on the other hand, Syt1 is typically known as an axon terminal-specific protein. In line with this, previous work in primary DA neurons failed to detect Syt1 immunoreactivity in the cell body and dendrites of DA neurons, with the protein detected in the vast majority of non-synaptic and synaptic terminals along DA neuron axons *(Mendez et al., 2011; Ducrot et al., 2021)*. One possibility is that part of the DA release detected in the VTA and SNc derives from local DA neuron axon collaterals, which would contain Syt1. However, very little solid anatomical data exists currently to support the existence of a large number of such local collaterals, although minimal quantitative data suggest that the VTA contain axonal collaterals arising from its own axons and from SNc DA neurons *(Deutch et al., 1988; Bayer and Pickel, 1990)*. To address this question more directly, we devised a new strategy to selectively activate the STD compartment of DA neurons using an optogenetic approach. For this, we expressed a Kv2.1-ChR2-YFP fusion construct in DA neurons that we showed was predominantly expressed in the STD compartment of DA neurons. While the expression of this ChR2 protein was purely STD in primary DA neurons, a small contingent of axons in the ventral striatum appeared to contain the protein. As optically-evoked DA release

in the ventral striatum of these mice was blocked by suppressing firing with TTX, we performed all experiments in ventral mesencephalic slices in the present of TTX, thus limiting any contribution of axonal processes to evoked DA release. We found that STD DA release was still detectable under such conditions and this STD DA release was not reduced by *syt1* gene deletion. Together, these results provide support for the fact that activity-dependent DA release detected in the VTA, and potentially also in the SNc, implicates a mix of STD and axonal DA release. A dual nature of released DA in the mesencephalon was also previously suggested based on an analysis of the calcium-dependency of DA release in the guinea pig VTA *(Chen et al., 2011)*, although other work has provided support for a similar calcium-dependency of release in mouse striatum and mesencephalon *(Beckstead et al., 2004, 2007; Courtney et al., 2012; Ford et al., 2009, 2010; Delignat-Lavaud et al., 2021)*. Because the available anatomical data suggests that DA containing axonal varicosities are extremely scarce in the SNc and VTA except in the context of compensatory axonal sprouting associated with partial lesions *(Fernandes Xavier et al., 1994)*, it would be important to revisit this question in the future with a more thorough anatomical investigation. The novel optogenetic approach described here in order to trigger STD DA release more selectively should be very useful in the future to further explore the distinct molecular machinery involved in STD and axonal DA release so as to extend recent work showing a role for Syt4 and Syt7 isoforms in this process *(Mendez et al., 2011; Delignat-Lavaud et al., 2021)*.

Considering that electrically evoked DA release in the VTA of Syt1 cKO^{DA} mice was reduced by approximately two-thirds, the near abolition of DA release in the VTA after the adult KO of Syt1 is a puzzling observation. Considering the suboptimal selectivity of the TH-Cre virus used, one obvious possibility is that this could be an artifact due to abrogation of neurotransmitter release from local non-DA neurons that are also stimulated by the extracellular electrodes and that contribute to triggering STD DA release. An approach to

resolve this would be to combine this adult KO strategy with the proposed STD optogenetic approach. The use of an inducible DAT-Cre line would also be another possibility to obtain a more selective adult Syt1 KO.

Our results shed new light on the striking resilience of DA-dependent motor functions at early stages of PD, during which an extensive loss of DA in the striatum gradually occurs with substantial motor dysfunctions only appearing after more than 70% of terminals in the striatum are lost *(Halliday et al., 1990)*. This resilience has been hypothesized to be due to gradually established compensations in the DA system, including increased DA synthesis in the remaining DA axons and D2 receptor upregulation, which has been observed in human tissue and in multiple PD models *(Bezard et al., 2003; Mercuri and Bernardi, 2005; Golden et al., 2013)*. Our work raises the hypothesis that as loss of DA terminals progresses in PD, even if phasic DA release is greatly impaired, as long as a sufficient tone of basal extracellular is maintained, many basic motor functions will be preserved. This may also help explain why even strategies that increase the basal tone of DA without restoring the normal connectivity of DA neurons, such as the implantation of DA-secreting non-neuronal cells can help to reduce motor symptoms in PD animal models *(Parmar et al., 2019)*. In this context, Syt1 cKO^{DA} mice could represent a new model to study compensatory mechanisms and sensitivity in PD.

This model also represents a new tool to study spontaneous release mechanisms and to tackle the role of phasic DA release in the brain. Evaluation of other DA-controlled functions such as motivation, learning, cognition or reward would be an important next step to further document the role of phasic DA release. Our findings are also likely to be relevant to a better understanding of signaling by other neuromodulators such as serotonin and norepinephrine, that show connectivity patterns that are similar to that of DA neurons.

Our results are also compatible with previous work obtained in mice in which 90% of SNc dopaminergic neurons were genetically ablated, leading to a consequent depletion of > 95% of striatal DA *(Golden et al., 2013)*. In these mice, motor behaviors of young-adult or aged mice were also largely unaltered. These mutant mice also exhibited an exaggerated response to L-DOPA suggesting that preservation of motor functions involves sensitization of striatal DA receptors. This result is in keeping with our amphetamine-induced locomotion and autoradiography results, which also point toward the sensitization of DA receptors in Syt1$^{-/-}$ mice. The authors concluded that <5% of striatal dopamine is sufficient to maintain basic motor functions. Similarly, our findings are in tune with previous work in which NMDA receptors were conditionally deleted from DA neurons *(Zweifel et al., 2009)*. In these mice, phasic DA release in the striatum was found partially impaired, but many DA-dependent behaviors, including unconditioned motor behaviors, were unaffected, while other conditioned behaviors were impaired (conditioned place preference, T-maze, and instrumental conditioning).

In summary, we conclude that although Syt1 is clearly the main calcium sensor controlling DA release, a small component of phasic DA release requires another calcium sensor. We also conclude that Syt1-dependent phasic DA release is dispensable for many basic unconditioned motor functions that require instead only a basal level of extracellular DA that could be provided either by (a) spontaneous DA exocytosis, (b) by the small component of phasic DA release that depends on other calcium sensors, (c) by phasic but desynchronized exocytosis or even (d) by DAT-mediated reverse transport. Further work will be required to test these possibilities.

Acknowledgements

We would like to thank Dr. R. Schneggenburger for kindly provided the Syt1-floxed mouse, Dr. J. Surmeier for kindly provided TH-cre and control viruses, Dr. G. Miller for kindly provided VMAT2 antibody, Dr. A. Gratton for interpretation of HPLC data and M-E. Delignat-Lavaud for illustrations. This work was funded by the National Sciences and Engineering Research Council of Canada (NSERC, grant RGPIN-2020-05279) to L-E.T. B.D-L received a graduate student award from Parkinson Canada.

Author contributions

B.D-L.: conceptualization and design, acquisition, analysis, validation and interpretation of data (voltammetry, behavior, autoradiography, IHC, viral infections and RT-qPCR), drafting or revising the manuscript. J.K.: acquisition and analysis of data (IHC). C.D.: acquisition and analysis of data (ICC). I.M.: acquisition and analysis of data (microdialysis). S.M..: acquisition and analysis of data (Western Blot). N.G.: acquisition and analysis of data (stereology), revising the manuscript. L.M.: acquisition of data (HPLC). C.L.: acquisition of data (autoradiography). S.B.N.: acquisition of data (ICC). M-J.: acquisition of data (cell culture), P. R-N.: review and editing, D.L.: review, editing and analysis of data (autoradiography), L. D.B.: review and editing, L-E.T.: conceptualization and design, resources, funding acquisition, writing - review and editing.

Declaration of interests

The authors declare that they have no conflicts of interest.

Figures and legend

Fig.1

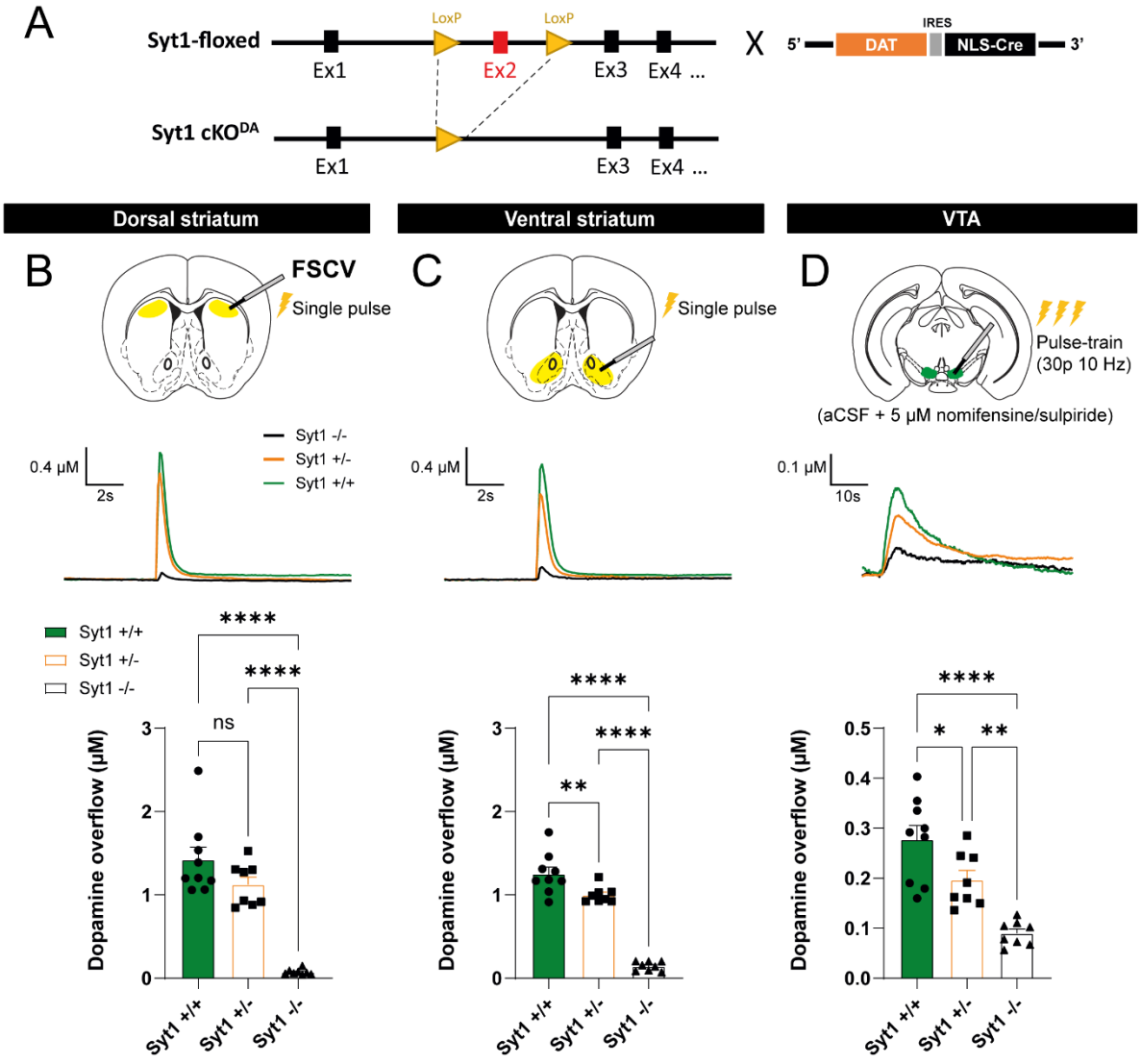

Figure 1: Syt1 is the main calcium sensor for fast axonal dopamine release. (A) *Generation of conditional knock-out of Syt1 in DA neurons by crossing Syt1-floxed mice (Syt1$^{lox/lox}$) with DAT^{IREScre} mice.* ***(B)*** *Fast scan cyclic recording of Syt1 cKO^{DA} mice in the dorsal striatum. Representative traces (top) and quantification of peak amplitude (bottom) obtained with single-pulse electrical stimulation (1 ms, 400 µA) in Syt1$^{+/+}$ (n = 18 slices/9 mice), Syt$^{+/-}$ (n = 16/8) and Syt1$^{-/-}$ mice (n = 16/8).* ***(C)*** *Same, but in the ventral striatum (NAc core and shell).* ***(D)*** *Representative traces (top) and quantification of peak amplitude (bottom) obtained in the VTA with aCSF containing nomifensine (DAT blocker) and sulpiride (D2 antagonist) (both at 5*

*µM), and pulse-train stimulation (30 pulses of 1 ms at 10 Hz, 400µA). Error bars represent ± S.E.M. and the statistical analysis was carried out by 1-way ANOVAs followed by Tukey tests (ns, non-significant; *, p < 0.05; **, p < 0.01; ***, p < 0.001; ****, p < 0.0001).*

Fig. 2

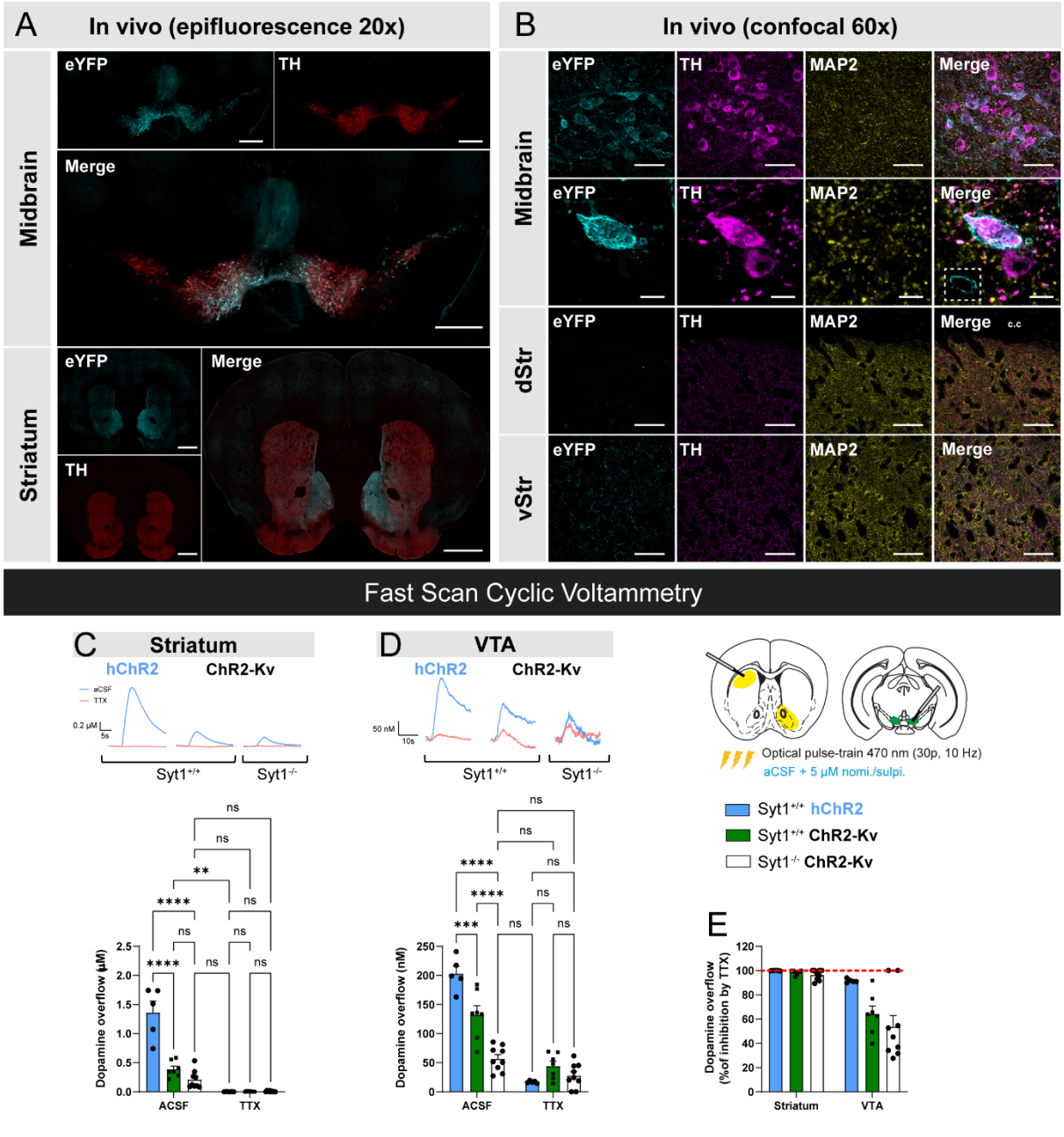

Figure 2: Somatodendritic optogenetics reveals unaltered STD DA release in the absence of Syt1. (A) *Immunohistochemistry in brain slices of adult Syt1 cKO^{DA} mice infected with AAV2/5-hsyn-DIO-ChR2-eYFP-Kv, showing expression of ChR2-Kv (eYFP) in the whole ventral*

mesencephalon (scale bar = 500 µm) and striatum (scale bar = 1 mm) using epifluorescence microscope at 20x. ***(B)*** *Expression of ChR2-Kv in the same mice evaluated by confocal microscopy at 60x shows infected DA neurons (TH) in the midbrain (up panel, scale bar = 50 µm). Optical zoom and z-stack on an infected DA neuron showing the membrane distribution of the eYFP signal (bottom panel, scale bar = 10 µm, insert in the merge image shows the eYFP signal at a single focal plane). Evaluation of the eYFP signal in the striatum shows no axonal processes in the dorsal sector but a small contingent of positive fibers in the ventral sector of the striatum (scale bar = 50 µm).* ***(C-E)*** *Fast scan cyclic voltammetry recordings with average [DA]o peaks obtained in striatal* ***(C)*** *and midbrain* ***(D)*** *slices of infected Syt1$^{+/+}$ and Syt1$^{-/-}$ mice with AAV2/5-hsyn-DIO-ChR2-eYFP-Kv (ChR2-Kv) or AAV5-EF1a-DIO-hChR2(H134R)-eYFP (control hChR2). Representative traces of each conditions are shown at the top. DA release was optically triggered in each region using pulse-train stimulation (30 pulses of 470 nm blue light at 10 Hz) in ACSF containing 5 µM of nomifensine and sulpiride.* ***(E)*** *TTX (1 µM) effect on average [DA]o peaks in the striatum and the VTA (% of inhibition).*

Fig.3

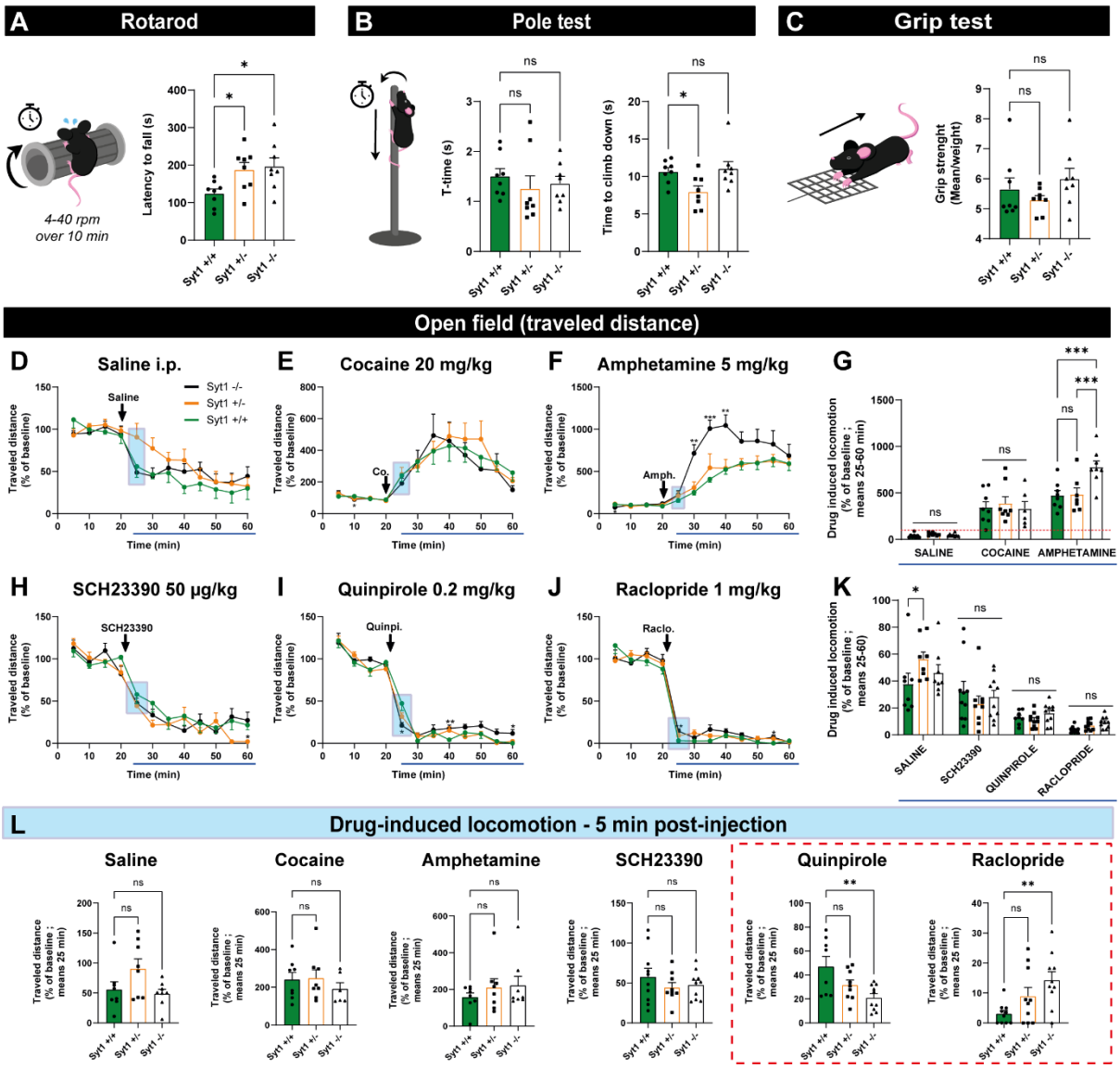

Figure 3: Syt1 cKO^{DA} mice do not exhibit any substantial motor defects. (A) *Latency to fall from the device during the rotarod test for Syt1$^{+/+}$, Syt1$^{+/-}$ and Syt1$^{-/-}$ mice (n = 8, mean of 3 attempts)* ***(B)*** *Time for Syt1$^{+/+}$, Syt1$^{+/-}$ and Syt1$^{-/-}$ mice (n = 8) to turn (t-turn) and climb down the vertical pole (mean of 3 attempts/2 days).* ***(C)*** *Forelimb grip strength (mean of 3 trials/weight) developed by Syt1$^{+/+}$, Syt1$^{+/-}$ and Syt1$^{-/-}$ mice (n = 8), using a force sensor connected to a grid. Statistical analysis for A-C were carried out by 1-way ANOVAs followed by Dunnett tests.* ***(D-L)*** *Locomotion of Syt1 cKO^{DA} mice measured as traveled distance (% of a 20 min baseline) under saline treatment (n = 8 mice)* ***(D)****, cocaine at 20 mg/kg (n = 8*

$Syt1^{+/+}$/$Syt1^{+/-}$ and 6 $Syt1^{-/-}$) ***(E)****, amphetamine at 5 mg/kg (n = 8 mice)* ***(F)****, the D1 agonist SCH23390 at 50 µg/kg (n = 10 $Syt1^{+/+}$/$Syt1^{-/-}$ and 9 $Syt1^{+/-}$)* ***(H)****, the D2 agonist quinpirole at 0.2 mg/kg (n = 10 $Syt1^{-/-}$ / $Sy^{+/-}$ and 8 $Syt1^{+/+}$)* ***(I)*** *and the D2 antagonist raclopride at 1 mg/kg (n = 10 mice)* ***(J)****. Statistical analyses for D-J were carried out by 2-way ANOVAs followed by Dunnett tests.* ***(G&K)*** *Average drug-induced locomotion (% of baseline) during a 40 min recording period (mean between 25-60 min) are represented for cocaine/amphetamine treatment* ***(G)*** *and for SCH23390/quinpirole/raclopride treatments* ***(K)****. Statistical analysis was carried out by 2-way ANOVAs followed by Tuckey tests. Blue squares indicate the average traveled distance for each mouse, 5 min after receiving an i.p. injection of each tested drugs* ***(L)****. Statistical analysis was carried out by 1-way ANOVAs followed by Dunnett tests. Error bars represent ± S.E.M. (ns, non-significant; *, $p < 0.05$; **, $p < 0.01$; ***, $p < 0.001$; ****, $p < 0.0001$).*

Fig.4

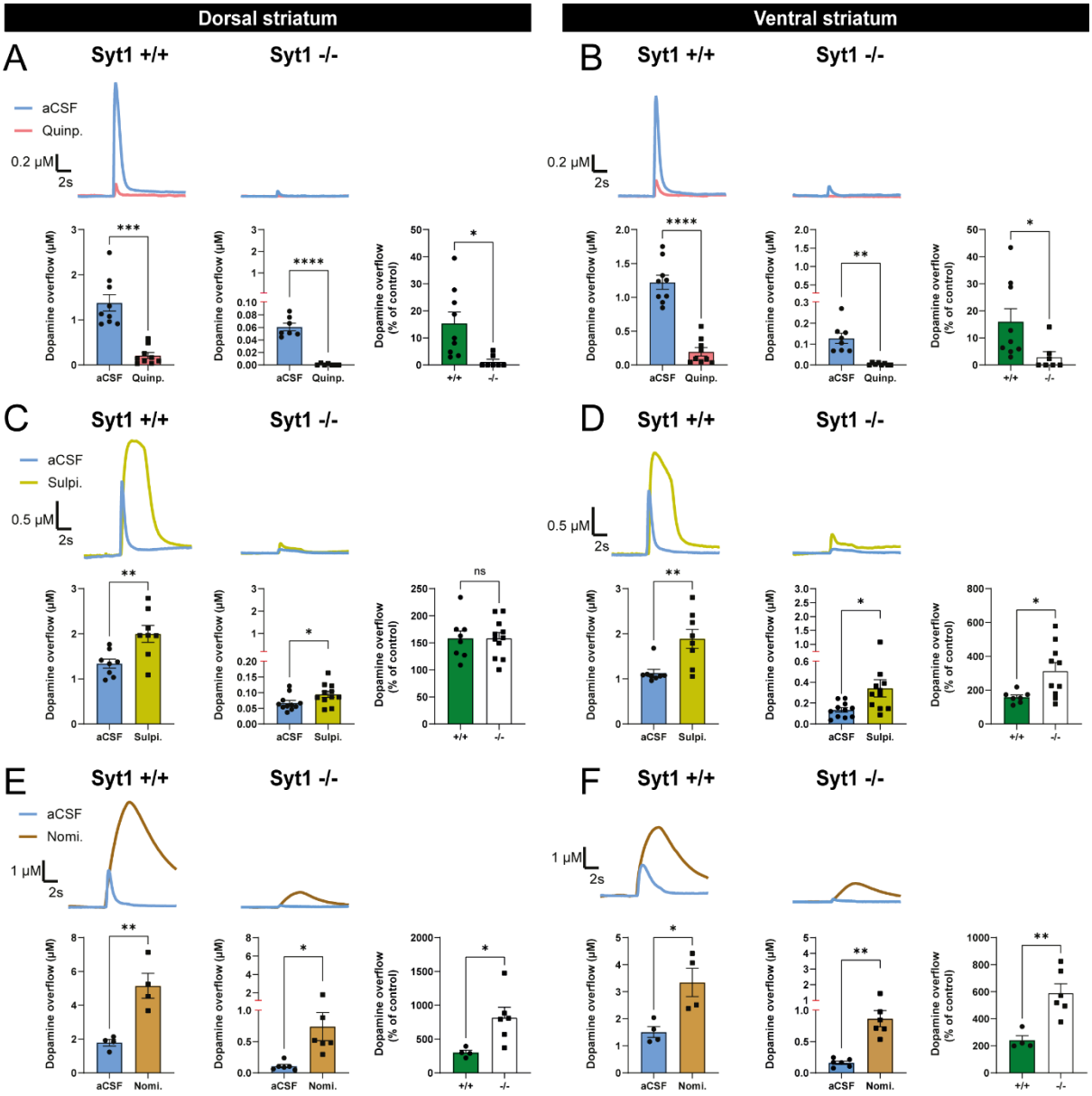

1031

1032 ***Figure 4:*** **Increased D2 autoreceptor and DAT function in Syt1 cKO^{DA} mice.** ***(A)*** *FSCV*
1033 *representative traces (top) and quantification of peak amplitude (bottom) obtained in Syt1$^{+/+}$*
1034 *and Syt1$^{-/-}$ mice with single-pulse electrical stimulation and aCSF containing 1 µM of the D2*
1035 *agonist quinpirole.* ***(B)*** *Same, but in the ventral striatum.* ***(C)*** *FSCV representative traces (top)*
1036 *and quantification of peak amplitude (bottom) obtained in Syt1$^{+/+}$ and Syt1$^{-/-}$ mice with pulse-*
1037 *train stimulation and aCSF containing 5 µM of the D2 antagonist sulpiride.* ***(D)*** *Same, but in*
1038 *the ventral striatum.* ***(E)*** *FSCV representative traces (top) and quantification of peak amplitude*

(bottom) obtained in Syt1$^{+/+}$ and Syt1$^{-/-}$ mice with pulse-train stimulation and aCSF containing 5 µM of the DAT blocker nomifensine. ***(F)*** *Same, but in the ventral striatum. For each tested drug, the effect on DA release (% of control) for both genotypes is indicated in the right panel. Statistical analysis was carried out by 2-way ANOVAs followed by Šidák's corrections. Error bars represent ± S.E.M. (ns, non-significant; *, p < 0.05; **, p < 0.01; ***, p < 0.001; ****, p < 0.0001).*

Fig.5

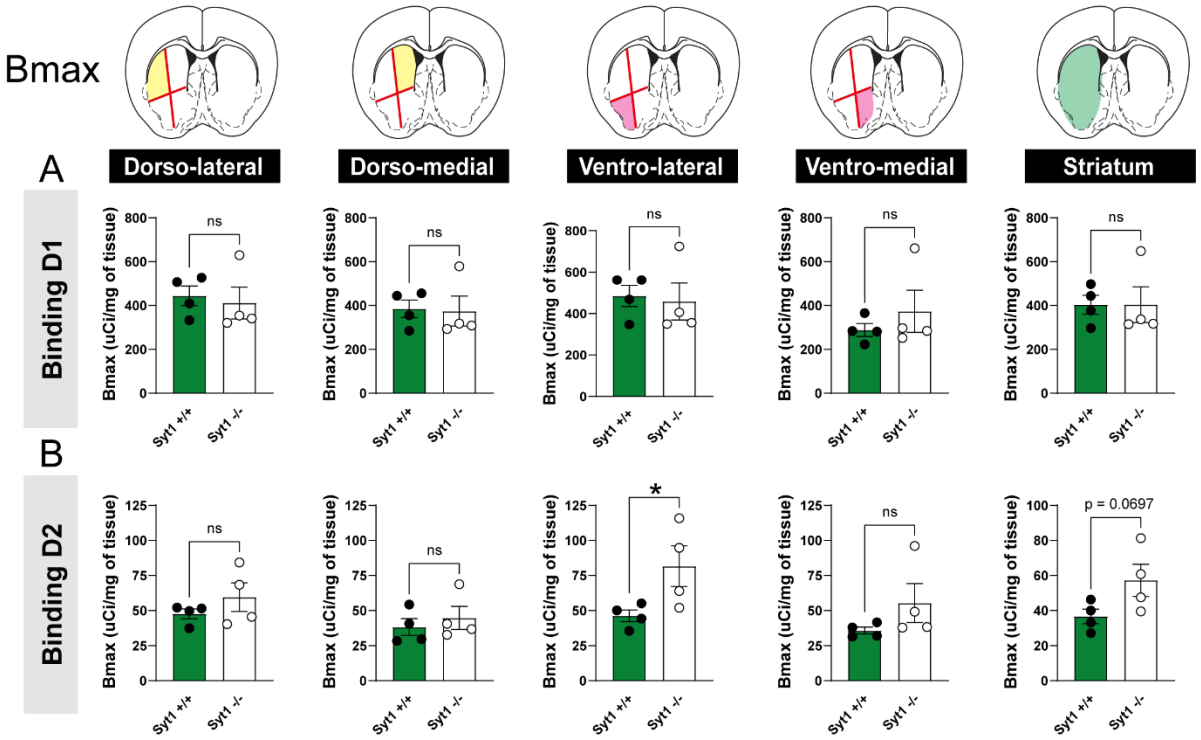

Figure 5: Higher D2 receptor density with no change in affinity in Syt1 cKO^{DA} mice. *Density of DA receptors (Bmax) for D1* ***(A)*** *and D2* ***(B)*** *in Syt1$^{+/+}$ and Syt1$^{-/-}$ mice (n = 4). Each binding was analyzed with a series of 4 serial coronal sections (bregma +1.34 mm to +0.38 mm) and by dividing each section into 4 quadrants (dorso-lateral, ventro-lateral, dorso-medial and ventro-medial). The data followed a log-normal distribution and unpaired t-tests were done after the data were converted to a log scale. Error bars represent ± S.E.M. (ns, non-significant; *, p < 0.05; **, p < 0.01; ***, p < 0.001; ****, p < 0.0001).*

Fig.6

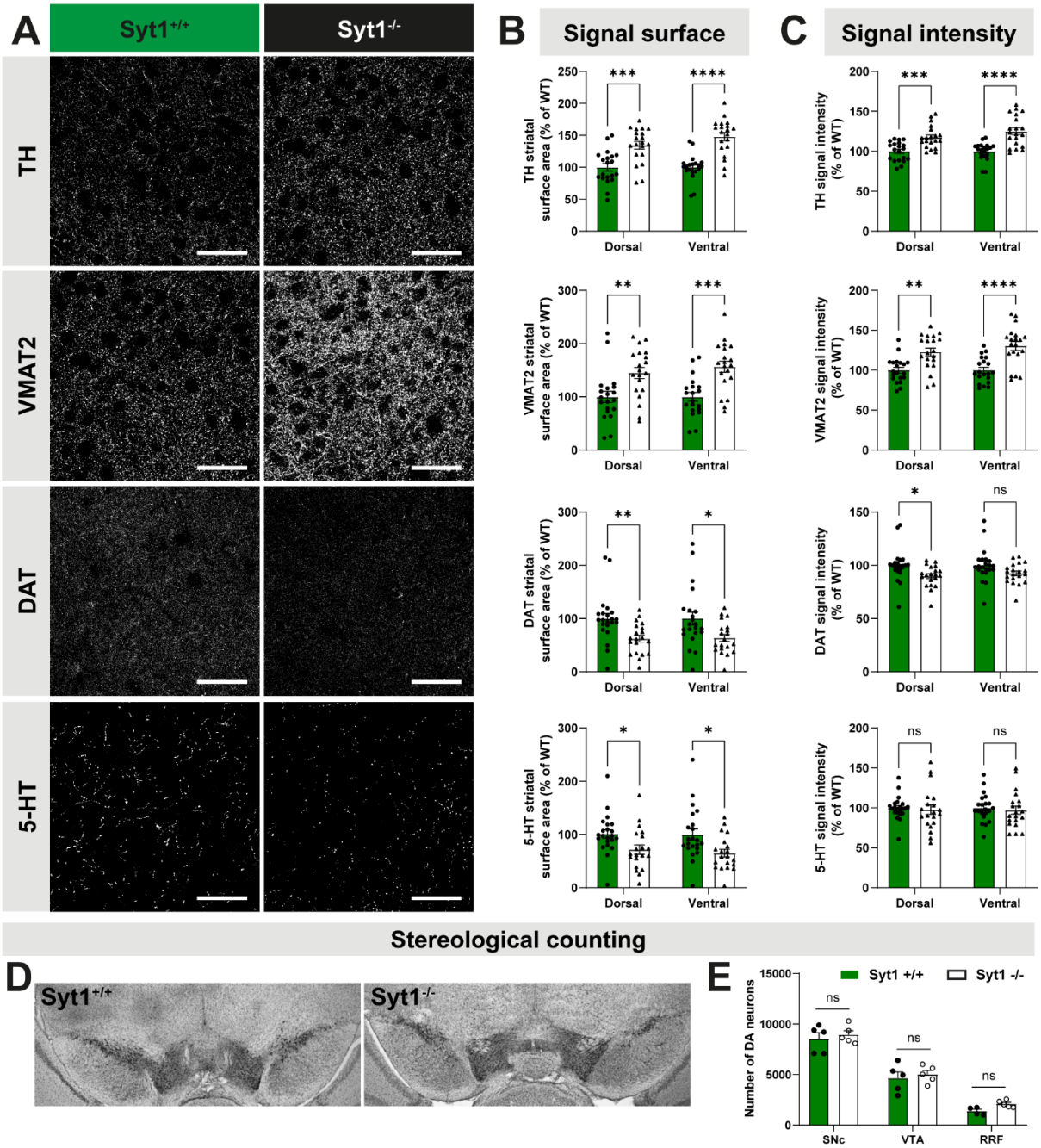

Figure 6: Adaptations of DA innervation in Syt1 cKO^{DA} mice. (A) *Immunochemistry of striatal slices from 10-12 week-old Syt1$^{+/+}$ and Syt1$^{-/-}$ mice (60x confocal) using (from top to bottom): tyrosine hydroxylase (TH), vesicular monoamine transporter 2 (VMAT2), dopamine transporter (DAT) and serotonin (5-HT) immunostainings. Scale bar = 50 µm.* ***(B)*** *Quantification of each signal surface (% of WT) in the dorsal and ventral striatum (n = 20 hemispheres/10 mice).* ***(C)*** *Same with signal intensity.* ***(D)*** *TH immunoreactive cells in the*

midbrain of Syt1$^{+/+}$ and Syt1$^{-/-}$ mice, identified by the brown DAB staining. ***(E)*** *Stereological counts of DA neurons in the SNc, VTA and RRF. Unbiased stereological counting was performed by a blinded observer to estimate the number of DA neurons. Statistical analysis was carried out by 2-way ANOVAs followed by Šidák's corrections. Error bars represent ± S.E.M. (ns, non-significant; *, $p < 0.05$; **, $p < 0.01$; ***, $p < 0.001$; ****, $p < 0.0001$).*

Fig.7

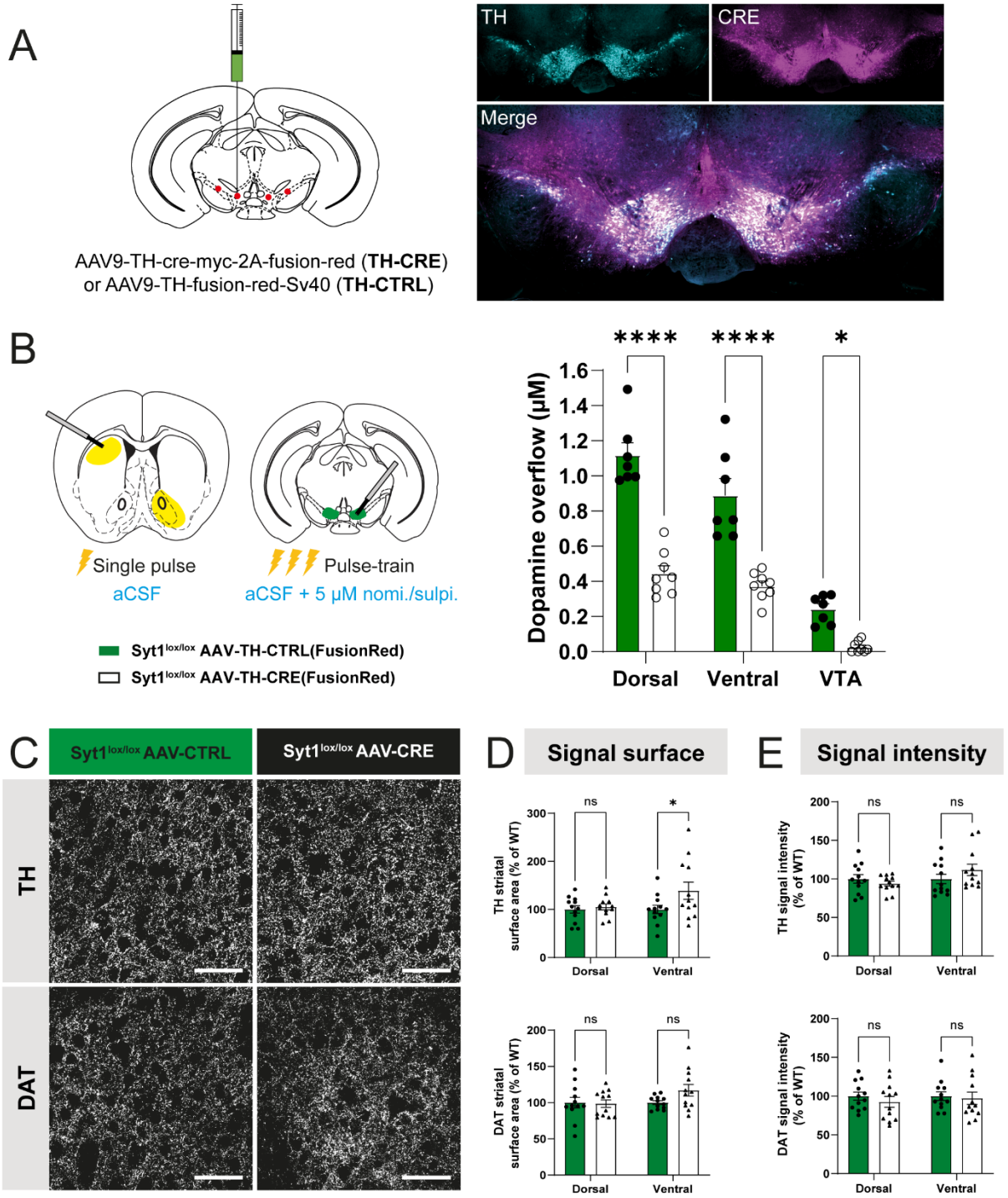

Figure 7: Acute deletion of Syt1 in adult mice impairs DA release but prevents adaptations. ***(A)*** *Stereotaxic injections of AAV9-TH-Cre and AAV9-TH-FusionRed (control) viruses in 6-7-week-old Syt1$^{lox/lox}$ mice effectively infects the whole ventral mesencephalon (epifluorescence imaging of TH (cyan) and FusionRed (Cre, magenta) immunostainings).* ***(B)*** *FSCV recordings*

(DA overflow in µM) of dorsal and ventral striatum (single electrical pulse 1 ms, 400 µA, normal aCSF) and VTA (pulse-train 30p, 1ms, 400 µA, 10 Hz in presence of 5 µM of nomifensine/sulpiride) from Syt1$^{lox/lox}$ mice injected with AAV9-TH-Cre and AAV9-TH-Control viruses. (C) Immunohistochemistry of striatal slices from 9-10 week old Syt1$^{lox/lox}$ injected with AAV9-TH-Cre (black) and AAV9-TH-control (green) illustrating TH and DAT immunostaining (60x confocal). Scale bar = 50 µm. ***(B)*** *Quantification of each signal surface (% of WT) in the dorsal and ventral striatum of injected mice (n = 12 hemispheres/6 mice).* ***(C)*** *Same with signal intensity. Statistical analysis was carried out by 2-way ANOVAs followed by Šidák's corrections. Error bars represent ± S.E.M. (ns, non-significant; *, p < 0.05; **, p < 0.01; ***, p < 0.001; ****, p < 0.0001).*

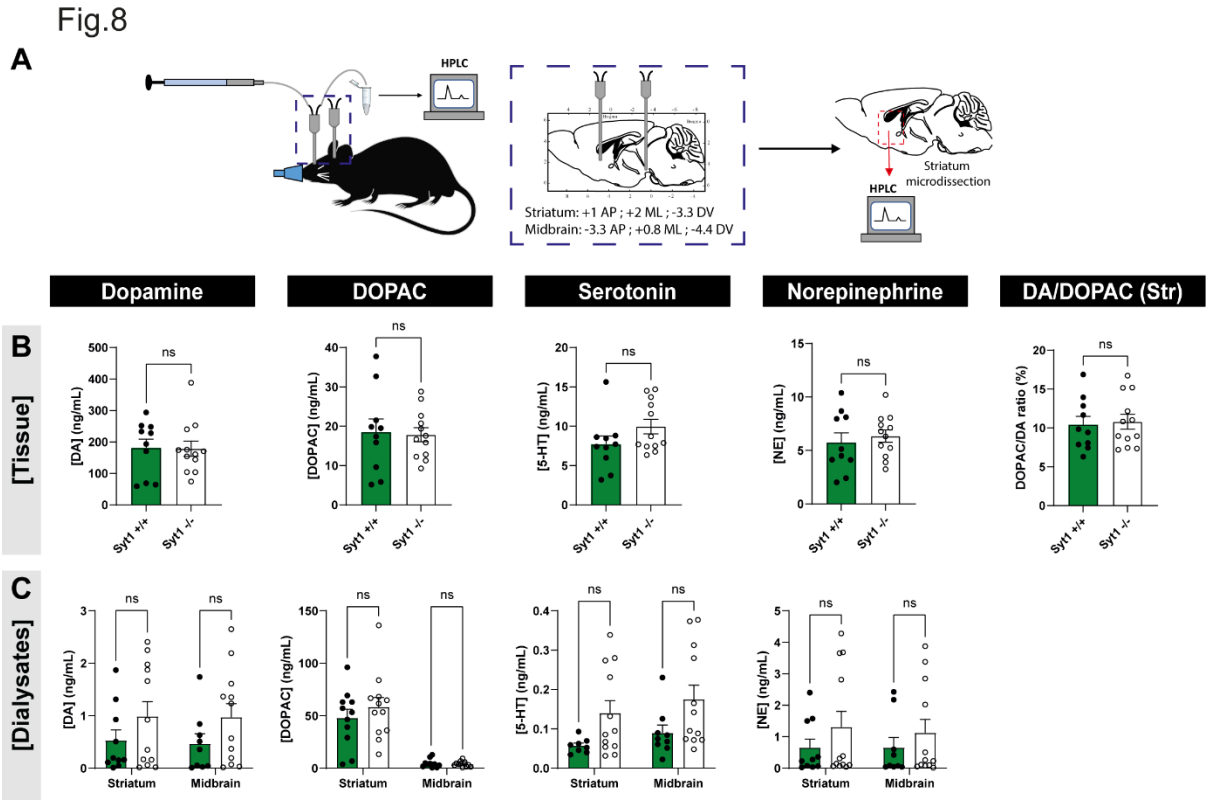

Figure 8: Basal extracellular DA levels and total tissue DA are not altered in Syt1 cKO^{DA} mice. (A) *Schematic representation of the intracerebral microdialysis protocol performed on*

anesthetized Syt1 cKO^{DA} and control mice. ***(B)*** *Quantification of total DA, DOPAC, serotonin and norepinephrine striatal content and DA/DOPAC ratio (n = 10 Syt1$^{+/+}$ and 12 Syt1$^{-/-}$). Statistical analysis was carried out by unpaired t-test.* ***(C)*** *Extracellular quantification by microdialysis of the same molecules in the dorsal striatum and in the mesencephalon of Syt1 cKO^{DA} mice, with an average of 3 dialysates for each animal. Statistical analysis was carried out by 2-way ANOVAs followed by Šidák's corrections. Error bars represent ± S.E.M. (ns, non-significant; *, $p < 0.05$; **, $p < 0.01$; ***, $p < 0.001$; ****, $p < 0.0001$).*

References

Andrews, N.W., Chakrabarti, S., 2005. There's more to life than neurotransmission: the regulation of exocytosis by synaptotagmin VII. Trends Cell Biol 15, 626–631. https://doi.org/10.1016/j.tcb.2005.09.001

Antonopoulos, J., Dori, I., Dinopoulos, A., Chiotelli, M., Parnavelas, J.G., 2002. Postnatal development of the dopaminergic system of the striatum in the rat. Neuroscience 110, 245–256. https://doi.org/10.1016/S0306-4522(01)00575-9

Bacaj, T., Wu, D., Burré, J., Malenka, R.C., Liu, X., Südhof, T.C., 2015. Synaptotagmin-1 and -7 Are Redundantly Essential for Maintaining the Capacity of the Readily-Releasable Pool of Synaptic Vesicles. PLOS Biology 13, e1002267. https://doi.org/10.1371/journal.pbio.1002267

Bacaj, T., Wu, D., Yang, X., Morishita, W., Zhou, P., Xu, W., Malenka, R.C., Südhof, T.C., 2013. Synaptotagmin-1 and Synaptotagmin-7 Trigger Synchronous and Asynchronous Phases of Neurotransmitter Release. Neuron 80, 947–959. https://doi.org/10.1016/j.neuron.2013.10.026

Baker, C.A., Elyada, Y.M., Parra, A., Bolton, M.M., n.d. Cellular resolution circuit mapping with temporal-focused excitation of soma-targeted channelrhodopsin. eLife 5, e14193. https://doi.org/10.7554/eLife.14193

Banerjee, A., Imig, C., Balakrishnan, K., Kershberg, L., Lipstein, N., Uronen, R.-L., Wang, J., Cai, X., Benseler, F., Rhee, J.S., Cooper, B.H., Liu, C., Wojcik, S.M., Brose, N., Kaeser, P.S., 2020a. Molecular and functional architecture of striatal dopamine release sites. bioRxiv 2020.11.25.398255. https://doi.org/10.1101/2020.11.25.398255

Banerjee, A., Lee, J., Nemcova, P., Liu, C., Kaeser, P.S., 2020b. Synaptotagmin-1 is the Ca2+ sensor for fast striatal dopamine release. eLife 9, e58359. https://doi.org/10.7554/eLife.58359

Bayer, V.E., Pickel, V.M., 1990. Ultrastructural localization of tyrosine hydroxylase in the rat ventral tegmental area: relationship between immunolabeling density and neuronal associations. J. Neurosci. 10, 2996–3013.

Beckstead, M.J., Ford, C.P., Phillips, P.E.M., Williams, J.T., 2007. Presynaptic regulation of dendrodendritic dopamine transmission. Eur. J. Neurosci. 26, 1479–1488. https://doi.org/10.1111/j.1460-9568.2007.05775.x

Beckstead, M.J., Grandy, D.K., Wickman, K., Williams, J.T., 2004. Vesicular dopamine release elicits an inhibitory postsynaptic current in midbrain dopamine neurons. Neuron 42, 939–946. https://doi.org/10.1016/j.neuron.2004.05.019

Bergquist, F., Niazi, H.S., Nissbrandt, H., 2002. Evidence for different exocytosis pathways in dendritic and terminal dopamine release in vivo. Brain Res. 950, 245–253. https://doi.org/10.1016/s0006-8993(02)03047-0

Bergquist, F., Shahabi, H.N., Nissbrandt, H., 2003. Somatodendritic dopamine release in rat substantia nigra influences motor performance on the accelerating rod. Brain Research 973, 81–91. https://doi.org/10.1016/S0006-8993(03)02555-1

Bezard, E., Gross, C.E., Brotchie, J.M., 2003. Presymptomatic compensation in Parkinson's disease is not dopamine-mediated. Trends in Neurosciences 26, 215–221. https://doi.org/10.1016/S0166-2236(03)00038-9

Carvelli, L., McDonald, P.W., Blakely, R.D., DeFelice, L.J., 2004. Dopamine transporters depolarize neurons by a channel mechanism. PNAS 101, 16046–16051. https://doi.org/10.1073/pnas.0403299101

Centonze, D., Grande, C., Saulle, E., Martín, A.B., Gubellini, P., Pavón, N., Pisani, A., Bernardi, G., Moratalla, R., Calabresi, P., 2003. Distinct Roles of D1 and D5 Dopamine Receptors in Motor Activity and Striatal Synaptic Plasticity. J Neurosci 23, 8506–8512. https://doi.org/10.1523/JNEUROSCI.23-24-08506.2003

Chen, B.T., Patel, J.C., Moran, K.A., Rice, M.E., 2011. Differential calcium dependence of axonal versus somatodendritic dopamine release, with characteristics of both in the ventral tegmental area. Front Syst Neurosci 5, 39. https://doi.org/10.3389/fnsys.2011.00039

Cliburn, R.A., Dunn, A.R., Stout, K.A., Hoffman, C.A., Lohr, K.M., Bernstein, A.I., Winokur, E.J., Burkett, J., Schmitz, Y., Caudle, W.M., Miller, G.W., 2017. Immunochemical localization of vesicular monoamine transporter 2 (VMAT2) in mouse brain. Journal of Chemical Neuroanatomy, Monoamine Transporters in Health and Disease 83–84, 82–90. https://doi.org/10.1016/j.jchemneu.2016.11.003

Courtney, N.A., Mamaligas, A.A., Ford, C.P., 2012. Species Differences in Somatodendritic Dopamine Transmission Determine D2-Autoreceptor-Mediated Inhibition of Ventral Tegmental Area Neuron Firing. J. Neurosci. 32, 13520–13528. https://doi.org/10.1523/JNEUROSCI.2745-12.2012

Delignat-Lavaud, B., Ducrot, C., Kouwenhoven, W., Feller, N., Trudeau, L.-É., 2021. Implication of synaptotagmins 4 and 7 in activity-dependent somatodendritic dopamine release. bioRxiv 2021.01.25.427983. https://doi.org/10.1101/2021.01.25.427983

Descarries, L., Bérubé-Carrière, N., Riad, M., Bo, G.D., Mendez, J.A., Trudeau, L.-É., 2008. Glutamate in dopamine neurons: Synaptic versus diffuse transmission. Brain Research Reviews, Basal Ganglia 58, 290–302. https://doi.org/10.1016/j.brainresrev.2007.10.005

Descarries, L., Watkins, K.C., Garcia, S., Bosler, O., Doucet, G., 1996. Dual character, asynaptic and synaptic, of the dopamine innervation in adult rat neostriatum: a quantitative autoradiographic and immunocytochemical analysis. J. Comp. Neurol. 375, 167–186. https://doi.org/10.1002/(SICI)1096-9861(19961111)375:2<167::AID-CNE1>3.0.CO;2-0

Deutch, A.Y., Goldstein, M., Baldino, F., Roth, R.H., 1988. Telencephalic projections of the A8 dopamine cell group. Ann. N. Y. Acad. Sci. 537, 27–50. https://doi.org/10.1111/j.1749-6632.1988.tb42095.x

Donnan, G.A., Woodhouse, D.G., Kaczmarczyk, S.J., Holder, J.E., Paxinos, G., Chilco, P.J., Churchyard, A.J., Kalnins, R.M., Fabinyi, G.C., Mendelsohn, F.A., 1991. Evidence for plasticity of the dopaminergic system in parkinsonism. Mol Neurobiol 5, 421–433. https://doi.org/10.1007/BF02935563

Dourado, M., Cardoso-Cruz, H., Monteiro, C., Galhardo, V., 2016. Effect of Motor Impairment on Analgesic Efficacy of Dopamine D2/3 Receptors in a Rat Model of Neuropathy. J Exp Neurosci 10, JEN.S36492. https://doi.org/10.4137/JEN.S36492

Ducrot, C., Bourque, M.-J., Delmas, C.V.L., Racine, A.-S., Bello, D.G., Delignat-Lavaud, B., Lycas, M.D., Fallon, A., Michaud-Tardif, C., Nanni, S.B., Herborg, F., Gether, U., Nanci, A., Takahashi, H., Parent, M., Trudeau, L.-E., 2021. Dopaminergic neurons establish a distinctive axonal arbor with a majority of non-synaptic terminals. The FASEB Journal 35, e21791. https://doi.org/10.1096/fj.202100201RR

Fasano, C., Bourque, M.-J., Lapointe, G., Leo, D., Thibault, D., Haber, M., Kortleven, C., Desgroseillers, L., Murai, K.K., Trudeau, L.-É., 2013. Dopamine facilitates dendritic spine formation by cultured striatal medium spiny neurons through both D1 and D2 dopamine receptors. Neuropharmacology 67, 432–443. https://doi.org/10.1016/j.neuropharm.2012.11.030

Fasano, C., Kortleven, C., Trudeau, L.-E., 2010. Chronic activation of the D2 autoreceptor inhibits both glutamate and dopamine synapse formation and alters the intrinsic properties of mesencephalic dopamine neurons in vitro. Eur J Neurosci 32, 1433–1441. https://doi.org/10.1111/j.1460-9568.2010.07397.x

Fasano, C., Poirier, A., DesGroseillers, L., Trudeau, L.-E., 2008. Chronic activation of the D2 dopamine autoreceptor inhibits synaptogenesis in mesencephalic dopaminergic neurons in vitro. Eur J Neurosci 28, 1480–1490. https://doi.org/10.1111/j.1460-9568.2008.06450.x

Fasano, Caroline, Thibault, D., Trudeau, L.-É., 2008. Culture of Postnatal Mesencephalic Dopamine Neurons on an Astrocyte Monolayer. Current Protocols in Neuroscience 44, 3.21.1-3.21.19. https://doi.org/10.1002/0471142301.ns0321s44

Fawaz, C.S., Martel, P., Leo, D., Trudeau, L.-E., 2009. Presynaptic action of neurotensin on dopamine release through inhibition of D2 receptor function. BMC Neuroscience 10, 96. https://doi.org/10.1186/1471-2202-10-96

Fernandes Xavier, F.G., Doucet, G., Geffard, M., Descarries, L., 1994. Dopamine neoinnervation in the substantia nigra and hyperinnervation in the interpeduncular nucleus of adult rat following neonatal cerebroventricular administration of 6-hydroxydopamine. Neuroscience 59, 77–87. https://doi.org/10.1016/0306-4522(94)90100-7

Ford, C.P., Gantz, S.C., Phillips, P.E.M., Williams, J.T., 2010. Control of extracellular dopamine at dendrite and axon terminals. J. Neurosci. 30, 6975–6983. https://doi.org/10.1523/JNEUROSCI.1020-10.2010

Ford, C.P., Phillips, P.E.M., Williams, J.T., 2009. The Time Course of Dopamine Transmission in the Ventral Tegmental Area. J. Neurosci. 29, 13344–13352. https://doi.org/10.1523/JNEUROSCI.3546-09.2009

Fortin, G.D., Desrosiers, C.C., Yamaguchi, N., Trudeau, L.E., 2006. Basal somatodendritic dopamine release requires snare proteins. J Neurochem 96, 1740–1749. https://doi.org/10.1111/j.1471-4159.2006.03699.x

Gagnon, D., Eid, L., Coudé, D., Whissel, C., Di Paolo, T., Parent, A., Parent, M., 2018. Evidence for Sprouting of Dopamine and Serotonin Axons in the Pallidum of Parkinsonian Monkeys. Front. Neuroanat. 12. https://doi.org/10.3389/fnana.2018.00038

Giguère, N., Delignat-Lavaud, B., Herborg, F., Voisin, A., Li, Y., Jacquemet, V., Anand-Srivastava, M., Gether, U., Giros, B., Trudeau, L.-É., 2019. Increased vulnerability of nigral dopamine neurons after expansion of their axonal arborization size through D2 dopamine receptor conditional knockout. PLOS Genetics 15, e1008352. https://doi.org/10.1371/journal.pgen.1008352

Golden, J.P., Demaro, J.A., Knoten, A., Hoshi, M., Pehek, E., Johnson, E.M., Gereau, R.W., Jain, S., 2013. Dopamine-dependent compensation maintains motor behavior in mice with developmental ablation of dopaminergic neurons. J. Neurosci. 33, 17095–17107. https://doi.org/10.1523/JNEUROSCI.0890-13.2013

Halliday, G.M., Li, Y.W., Blumbergs, P.C., Joh, T.H., Cotton, R.G.H., Howe, P.R.C., Blessing, W.W., Geffen, L.B., 1990. Neuropathology of immunohistochemically identified brainstem neurons in Parkinson's disease. Annals of Neurology 27, 373–385. https://doi.org/10.1002/ana.410270405

Hauber, W., 1996. Impairments of movement initiation and execution induced by a blockade of dopamine D1 or D2 receptors are reversed by a blockade of N-methyl-D-aspartate receptors. Neuroscience 73, 121–130. https://doi.org/10.1016/0306-4522(96)00036-x

Hikima, T., Lee, C.R., Witkovsky, P., Chesler, J., Ichtchenko, K., Rice, M.E., 2021. Activity-dependent somatodendritic dopamine release in the substantia nigra autoinhibits the releasing neuron. Cell Rep 35, 108951. https://doi.org/10.1016/j.celrep.2021.108951

Isingrini, E., Guinaudie, C., C Perret, L., Rainer, Q., Moquin, L., Gratton, A., Giros, B., 2017. Genetic elimination of dopamine vesicular stocks in the nigrostriatal pathway replicates Parkinson's disease motor symptoms without neuronal degeneration in adult mice. Sci Rep 7. https://doi.org/10.1038/s41598-017-12810-9

Itzhak, Y., Martin, J.L., 1999. Effects of cocaine, nicotine, dizocipline and alcohol on mice locomotor activity: cocaine–alcohol cross-sensitization involves upregulation of striatal dopamine transporter binding sites. Brain Research 818, 204–211. https://doi.org/10.1016/S0006-8993(98)01260-8

Jensen, C.S., Watanabe, S., Stas, J.I., Klaphaak, J., Yamane, A., Schmitt, N., Olesen, S.-P., Trimmer, J.S., Rasmussen, H.B., Misonou, H., 2017. Trafficking of Kv2.1 Channels to the Axon Initial Segment by a Novel Nonconventional Secretory Pathway. J Neurosci 37, 11523–11536. https://doi.org/10.1523/JNEUROSCI.3510-16.2017

Joshua, M., Adler, A., Bergman, H., 2009. The dynamics of dopamine in control of motor behavior. Current Opinion in Neurobiology, Motor systems • Neurology of behaviour 19, 615–620. https://doi.org/10.1016/j.conb.2009.10.001

Juraska, J.M., Wilson, C.J., Groves, P.M., 1977. The substantia nigra of the rat: a Golgi study. J. Comp. Neurol. 172, 585–600. https://doi.org/10.1002/cne.901720403

Kochubey, O., Babai, N., Schneggenburger, R., 2016. A Synaptotagmin Isoform Switch during the Development of an Identified CNS Synapse. Neuron 90, 984–999. https://doi.org/10.1016/j.neuron.2016.04.038

Lim, S.T., Antonucci, D.E., Scannevin, R.H., Trimmer, J.S., 2000. A novel targeting signal for proximal clustering of the Kv2.1 K+ channel in hippocampal neurons. Neuron 25, 385–397. https://doi.org/10.1016/s0896-6273(00)80902-2

Liu, C., Goel, P., Kaeser, P.S., 2021. Spatial and temporal scales of dopamine transmission. Nature Reviews Neuroscience 1–14. https://doi.org/10.1038/s41583-021-00455-7

Liu, C., Kershberg, L., Wang, J., Schneeberger, S., Kaeser, P.S., 2018. Dopamine Secretion Is Mediated by Sparse Active Zone-like Release Sites. Cell 172, 706-718.e15. https://doi.org/10.1016/j.cell.2018.01.008

Matsuda, W., Furuta, T., Nakamura, K.C., Hioki, H., Fujiyama, F., Arai, R., Kaneko, T., 2009. Single Nigrostriatal Dopaminergic Neurons Form Widely Spread and Highly Dense Axonal Arborizations in the Neostriatum. J. Neurosci. 29, 444–453. https://doi.org/10.1523/JNEUROSCI.4029-08.2009

Maximov, A., Lao, Y., Li, H., Chen, X., Rizo, J., Sørensen, J.B., Südhof, T.C., 2008. Genetic analysis of synaptotagmin-7 function in synaptic vesicle exocytosis. PNAS 105, 3986–3991. https://doi.org/10.1073/pnas.0712372105

Mendez, J.A., Bourque, M.-J., Fasano, C., Kortleven, C., Trudeau, L.-E., 2011. Somatodendritic Dopamine Release Requires Synaptotagmin 4 and 7 and the Participation of Voltage-gated Calcium Channels. J. Biol. Chem. 286, 23928–23937. https://doi.org/10.1074/jbc.M111.218032

Mercuri, N.B., Bernardi, G., 2005. The 'magic' of l-dopa: why is it the gold standard Parkinson's disease therapy? Trends in Pharmacological Sciences 26, 341–344. https://doi.org/10.1016/j.tips.2005.05.002

Misonou, H., Mohapatra, D.P., Trimmer, J.S., 2005. Kv2.1: A Voltage-Gated K+ Channel Critical to Dynamic Control of Neuronal Excitability. NeuroToxicology, First International Porto Pirgos Conference on Advances in Neuroscience 26, 743–752. https://doi.org/10.1016/j.neuro.2005.02.003

O'Neill, B., Patel, J.C., Rice, M.E., 2017. Characterization of Optically and Electrically Evoked Dopamine Release in Striatal Slices from Digenic Knock-in Mice with DAT-Driven Expression of Channelrhodopsin. ACS Chem Neurosci 8, 310–319. https://doi.org/10.1021/acschemneuro.6b00300

Ovsepian, S.V., Dolly, J.O., 2011. Dendritic SNAREs add a new twist to the old neuron theory. PNAS 108, 19113–19120. https://doi.org/10.1073/pnas.1017235108

Palij, P., Bull, D.R., Sheehan, M.J., Millar, J., Stamford, J., Kruk, Z.L., Humphrey, P.P., 1990. Presynaptic regulation of dopamine release in corpus striatum monitored in vitro in real time by fast cyclic voltammetry. Brain Res 509, 172–174. https://doi.org/10.1016/0006-8993(90)90329-a

Pang, Z.P., Bacaj, T., Yang, X., Zhou, P., Xu, W., Südhof, T.C., 2011. Doc2 supports spontaneous synaptic transmission by a Ca2+-independent mechanism. Neuron 70, 244–251. https://doi.org/10.1016/j.neuron.2011.03.011

Parish, C.L., Finkelstein, D.I., Drago, J., Borrelli, E., Horne, M.K., 2001. The role of dopamine receptors in regulating the size of axonal arbors. J Neurosci 21, 5147–5157.

Parish, C.L., Stanic, D., Drago, J., Borrelli, E., Finkelstein, D.I., Horne, M.K., 2002. Effects of long-term treatment with dopamine receptor agonists and antagonists on terminal arbor size. European Journal of Neuroscience 16, 787–794. https://doi.org/10.1046/j.1460-9568.2002.02132.x

Parmar, M., Torper, O., Drouin-Ouellet, J., 2019. Cell-based therapy for Parkinson's disease: A journey through decades toward the light side of the Force. Eur. J. Neurosci. 49, 463–471. https://doi.org/10.1111/ejn.14109

Paxinos and Franklin's the Mouse Brain in Stereotaxic Coordinates, Compact - 5th Edition [WWW Document], n.d. URL https://www.elsevier.com/books/paxinos-and-franklins-the-mouse-brain-in-stereotaxic-coordinates-compact/franklin/978-0-12-816159-3 (accessed 5.6.21).

Radl, D., Chiacchiaretta, M., Lewis, R.G., Brami-Cherrier, K., Arcuri, L., Borrelli, E., 2018. Differential regulation of striatal motor behavior and related cellular responses by dopamine D2L and D2S isoforms. PNAS 115, 198–203. https://doi.org/10.1073/pnas.1717194115

Rice, M.E., Patel, J.C., 2015. Somatodendritic dopamine release: recent mechanistic insights. Philos. Trans. R. Soc. Lond., B, Biol. Sci. 370. https://doi.org/10.1098/rstb.2014.0185

Richard, M.G., Bennett, J.P., 1994. Regulation by D2 dopamine receptors of in vivo dopamine synthesis in striata of rats and mice with experimental parkinsonism. Exp Neurol 129, 57–63. https://doi.org/10.1006/exnr.1994.1146

Robinson, B.G., Cai, X., Wang, J., Bunzow, J.R., Williams, J.T., Kaeser, P.S., 2019. RIM is essential for stimulated but not spontaneous somatodendritic dopamine release in the midbrain. eLife 8, e47972. https://doi.org/10.7554/eLife.47972

Schultz, W., 2007. Multiple Dopamine Functions at Different Time Courses. Annu. Rev. Neurosci. 30, 259–288. https://doi.org/10.1146/annurev.neuro.28.061604.135722

Stamford, J.A., Kruk, Z.L., Millar, J., 1988. Actions of dopamine antagonists on stimulated striatal and limbic dopamine release: an in vivo voltammetric study. Br J Pharmacol 94, 924–932. https://doi.org/10.1111/j.1476-5381.1988.tb11605.x

Steinkellner, T., Mus, L., Eisenrauch, B., Constantinescu, A., Leo, D., Konrad, L., Rickhag, M., Sørensen, G., Efimova, E.V., Kong, E., Willeit, M., Sotnikova, T.D., Kudlacek, O., Gether, U., Freissmuth, M., Pollak, D.D., Gainetdinov, R.R., Sitte, H.H., 2014. In Vivo Amphetamine Action is Contingent on α CaMKII. Neuropsychopharmacol 39, 2681–2693. https://doi.org/10.1038/npp.2014.124

Sudhof, T.C., 2004. The synaptic vesicle cycle. Annu. Rev. Neurosci. 27, 509–547. https://doi.org/10.1146/annurev.neuro.26.041002.131412

Sulzer, D., Sonders, M.S., Poulsen, N.W., Galli, A., 2005. Mechanisms of neurotransmitter release by amphetamines: a review. Prog. Neurobiol. 75, 406–433. https://doi.org/10.1016/j.pneurobio.2005.04.003

Surmeier, D.J., Graves, S.M., Shen, W., 2014. Dopaminergic modulation of striatal networks in health and Parkinson's disease. Curr Opin Neurobiol 29, 109–117. https://doi.org/10.1016/j.conb.2014.07.008

Tripanichkul, W., Stanic, D., Drago, J., Finkelstein, D.I., Horne, M.K., 2003. D2 Dopamine receptor blockade results in sprouting of DA axons in the intact animal but prevents sprouting following nigral lesions. Eur J Neurosci 17, 1033–1045. https://doi.org/10.1046/j.1460-9568.2003.02547.x

Wang, C., Kang, X., Zhou, L., Chai, Z., Wu, Q., Huang, R., Xu, H., Hu, M., Sun, X., Sun, S., Li, J., Jiao, R., Zuo, P., Zheng, L., Yue, Z., Zhou, Z., 2018. Synaptotagmin-11 is a critical mediator of parkin-linked neurotoxicity and Parkinson's disease-like pathology. Nat Commun 9, 1–14. https://doi.org/10.1038/s41467-017-02593-y

Ward, K.M., Citrome, L., 2018. Antipsychotic-Related Movement Disorders: Drug-Induced Parkinsonism vs. Tardive Dyskinesia—Key Differences in Pathophysiology and Clinical Management. Neurol Ther 7, 233–248. https://doi.org/10.1007/s40120-018-0105-0

Wassef, M., Berod, A., Sotelo, C., 1981. Dopaminergic dendrites in the pars reticulata of the rat substantia nigra and their striatal input. combined immunocytochemical localization of tyrosine hydroxylase and anterograde degeneration. Neuroscience 6, 2125–2139. https://doi.org/10.1016/0306-4522(81)90003-8

Xu, J., Mashimo, T., Südhof, T.C., 2007. Synaptotagmin-1, -2, and -9: Ca(2+) sensors for fast release that specify distinct presynaptic properties in subsets of neurons. Neuron 54, 567–581. https://doi.org/10.1016/j.neuron.2007.05.004

Zweifel, L.S., Parker, J.G., Lobb, C.J., Rainwater, A., Wall, V.Z., Fadok, J.P., Darvas, M., Kim, M.J., Mizumori, S.J.Y., Paladini, C.A., Phillips, P.E.M., Palmiter, R.D., 2009. Disruption of NMDAR-dependent burst firing by dopamine neurons provides selective assessment of phasic dopamine-dependent behavior. Proc Natl Acad Sci U S A 106, 7281–7288. https://doi.org/10.1073/pnas.0813415106